Electric Field Effect on Skyrmion phase in Chiral lattice Ferrimagnet Cu_2OSeO_3

Integrated Master of Science Thesis
Submitted by
Naman Agarwal

June 2016-December 2016

Thesis Adviser
Prof Henrik Rønnow
Laboratory of Quantum Magnetism(LQM)
EPFL,Lausanne, Switzerland

École Polytechnique Fédérale de Lausanne,

UM-DAE Centre for Excellence in Basic Sciences, Mumbai

External Examiner's Name

Thesis Adviser Signature   External Examiner's Signature

Wings are a constraint that makes
it possible to fly.
— Robert Bringhurst

To my parents...

Acknowledgements

I would first like to thank my thesis advisor Professor Henrik Ronnow at Laboratory of Quantum magnetism (LQM) at EPFL for giving me this opportunity to work under his guidance. Professor Ronnow offered me his immense support and is continuing source of inspiration for me. I am truly indebted to him for allowing me to be a part of his lab. I would also like to extend my sincere gratitude to Dr. Ivica Zivkovic for his continued support during experimental measurements . His guidance helped me in all the time of research and writing of this thesis. I would also like to extend my gratitude to fellow group member Huang Ping for the stimulating discussions and precious support in understanding the experimental setup and measurement technique which guided me through this study.

I would also like to acknowledge members of the Electronics workshop, mechanical workshop and PCB design workshop for invaluable discussions about material and design aspects and for their support in designing the setup within short time.

I would like to express my sincere gratitude to my institute and thesis coordinators Dr. Brijesh Prithvi and Dr. Manojendu Choudhury for supporting me during my time in Switzerland, being patient with me and for providing the freedom to complete this thesis.

I also like to thank my colleague at CBS as well as at EPFL, Akshay Koottandavida, for his kind support.

Finally, I express my gratitude to my parents, my classmates and my friends for their unfailing support and continuous encouragement throughout the duration of this study. This accomplishment would not have been possible without them. Thank you.

Lausanne, 15 December 2016   Naman Agarwal

Abstract

Insulator materials are the recent research interest in Spintronics because of the absence of joule heating. There has been continued interest in insulator material Cu_2OSeO_3 because it possesses the novel Skyrmion phase [1], specific type of spin vortices in the lattice, characterized by quantized topological number, near the paramagnetic phase boundary [2]. This Skyrmion phase can be harnessed for the switching applications in the data storage devices [3–6]. We study the effect of positive or negative DC electric field on the Skyrmion phase boundary of this material by magnetoelectric susceptibility(dM/dE) measurements, which is a sensitive technique for scanning phase boundary [7, 8]. We scan out the phase diagram for positive, negative and zero DC electric fields and find that electric field effect is maximum at the phase boundaries and decreases inside the phase There is no cut-off for the electric field effect. Also, the electric field effect is maximum at upper skyrmion boundary compared to other phase boundaries. We also show the small expansion(contraction) of Skyrmion phase along temperature axis with the application of positive(negative) DC electric field.

Key words: Skyrmions, Chiral ferromagnets, Magnetoelectric Susceptibility, Magnetoelectric couplings, DC electric field effect, Dzyaloshinskii-Moriya(DM) interactions, Ferromagnetic exchange interactions

Contents

Contents

List of Figures

Introduction

Magnetic ordering in the materials has been studied since quite long. We are familiar with different types of magnetic phases. Ferromagnetic, Ferrimagnetic, Antiferromagnetic and paramagnetic phases are quite well known.

We know that the magnetic materials have the great potential in the data storage devices for the switching applications because they can be tuned to have multiple stable states which can represent data bits. These stable states can be created by different kind of external forces like magnetic field, electric field or even pressure. The magnetic materials having magnetolectric coupling present a new way of manipulating the spins and hence the magnetic structure through electric field [9]. The tuning of spin structure using electric field presents an inexpensive and simple way of a writing the data bits in the device. Though much more needs to be done to make such devices practical in future applications.

Further tuning the magnetic metals using electric current presents another problem of Joule heating which can restrict the proper functioning of device and can affect the speed of data storage device. In this regard, magnetic insulator materials show a new hope in the area of spintronics because there are very small currents in these materials and thus there is no joule heating.

The magnetic insulator material Cu_2OSeO_3 has been a topic of recent interest because of its novel phase, Skyrmion phase [1], which can be accessed by small magnetic field. Having the phase transition temperature around 59 K, this material can't be used in practical applications. But it will definitely be able to give new insight to the physics which is yet unexplored.
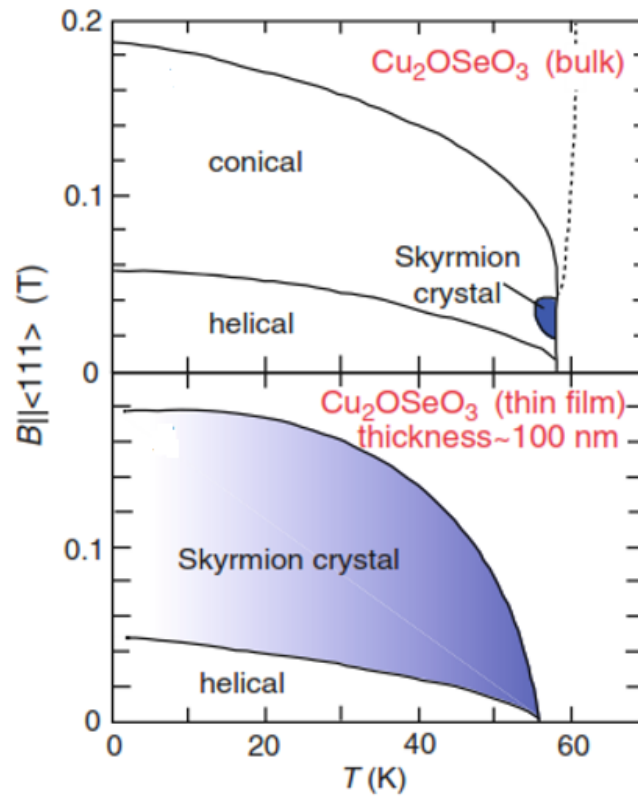
Figure 1 – Phase diagrams showing different phases and phase boundaries in bulk and thin film samples of Cu_2OSeO_3, [2]

In the present thesis, we seek the possibility of manipulating this skyrmion phase in Cu_2OSeO_3 by applying the external DC electric field [10, 11] and using the novel measurement technique, magnetoelectric susceptibility.

0.0.1 Construction of thesis

Chapter 1 describes the formation of magnetic skyrmions in general and in Cu_2OSeO_3. We take a look on the crystal structure of Cu_2OSeO_3 . Further I present some simulations showing the magnetoelectric response of Cu_2OSeO_3.

Chapter 2 describes the Experimental technique (magnetolectric susceptibility) used to do the measurements.

Chapter 3 describes the experimental setup for low temperature magnetic measurements and design of the sample probe and circuit for applying high voltage to the sample.

Chapter4 describes the magnetization and Magnetoelectric susceptibility Measurements done in this thesis project.

Chapter 5 addresses the important outcomes of this study and also summarizes some problems which need to be addressed in future.

1 Theory and Simulations

In this chapter, I will discuss about Skyrmions, origin of Skyrmion phase in Cu_2OSeO_3 and origin of skyrmions in general in other materials. Then I will present some simulations relating to onset of polarization in Cu_2OSeO_3 by application of magnetic field along different orientation as done in [12].

1.1 Skyrmions

Skyrmions were originally proposed by Tony Skyrme in 1960 in the context of particle physics. In condensed matter physics, their realization was proposed by Bogdanov in Chiral lattice ferromagnets due to lack of spatial inversion symmetry.

Magnetic Skyrmions are spin structures wrapped all around the sphere like a hedgehog as shown in the figure-1.1.

They represent vortex like spin structures having collective behavior. They are characterized by quantized topological number. Skyrmions are topologically protected.

1.1.1 Stabilization of Magnetic Skyrmions

There may be different mechanisms responsible for skyrmion formation in the magnets. I will describe two important mechanisms responsible for skyrmion formation [2].

First important mechanism is the competition between Dzyaloshinskii-Moriya(DM) and Ferromagnetic exchange interactions. In chiral lattice ferromagnets with broken spatial inversion symmetry, such as B20 compounds (MnSi, FeGe) and copper oxoselenite (Cu_2OSeO_3),the DM interactions originates from relativistic spin orbit coupling and favors the rotating alignment of spins with the turn angle of 90^0.whereas ferromagnetic exchange interaction favors the collinear ferromagnetic spin alignment. As a result of competition between these two interactions, helical spin order is formed in the absence of magnetic field. With the appli-
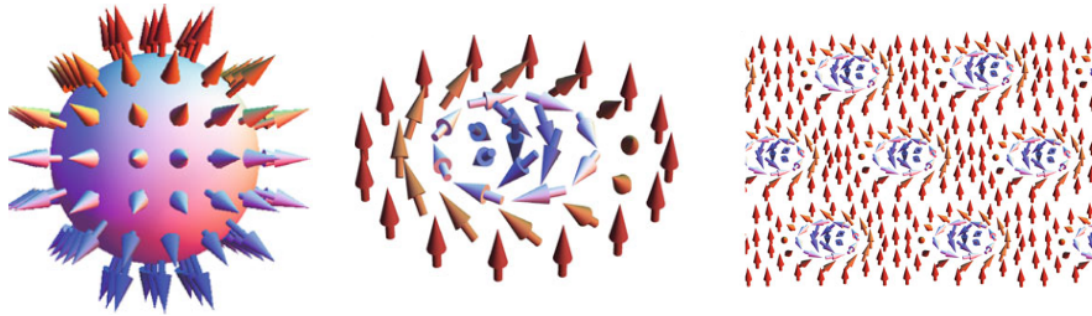
Figure 1.1 – Schematic of the original hedgehog-type skyrmion proposed by Tony Skyrme in the 1960s, whose magnetisations point in all directions wrapping a sphere. Schematic of a skyrmion recently discovered in chiral-lattice magnets, which corresponds to a projection of the hedgehog type skyrmion on a two-dimensional (2D) plane. Its magnetizations also point in all directions wrapping a sphere.Schematic of the skyrmion crystal realized in chiral-lattice magnets under an external magnetic field in which skyrmions are hexagonally packed to form a triangular lattice. [2]

cation of weak magnetic field, Skyrmions are formed in the plane perpendicular to applied field. As shown in figure 1.1,in skyrmions, magnetization is parallel to applied magnetic field at its periphery and anti-parallel at the center.Typically, Skyrmions unit cell is 3-100 nm in size in chiral lattice ferromagnets [2].The size of skyrmion lattice cell in these compounds is determined by a ratio of DM interaction and ferromagnetic exchange interaction.

Second major mechanism for skyrmion formation is competition between magnetic dipole interaction and easy axis anisotropy.The easy axis anisotropy favors out of plane magnetization whereas long range magnetic dipole interactions favor in plane magnetizations. The competition between two leads to periodic stripe with spins rotating in the plane in the absence of magnetic field. As the magnetic field is applied, the spin structures rearrange themselves to form skyrmions. This is important mechanism of Skyrmion formation for thin films of ferromagnets. The skyrmion unit cell formed in this case is 3-100 μm in size [2].

1.1.2 Skyrmions and Cu_2OSeO_3

As earlier described, the skyrmion formation in Cu_2OSeO_3 takes place due to competition between DM interaction and ferromagnetic interaction. Skyrmions in Cu_2OSeO_3 were first discovered by S.Seki et al. in 2012 [1].

The crystal structure of Cu_2OSeO_3 is shown in the figure 1.2.

The crystal lattice is characterized by space group $P2_13$. In Cu_2OSeO_3, there are two different Cu^2 sites in terms of spin alignment, in the ration of 3:1 This gives local ferromagnetic ordering with 3-up and 1-down type spin configuration.Helical phase is formed in the ground state whereas application of small magnetic field near the critical temperature leads to formation of
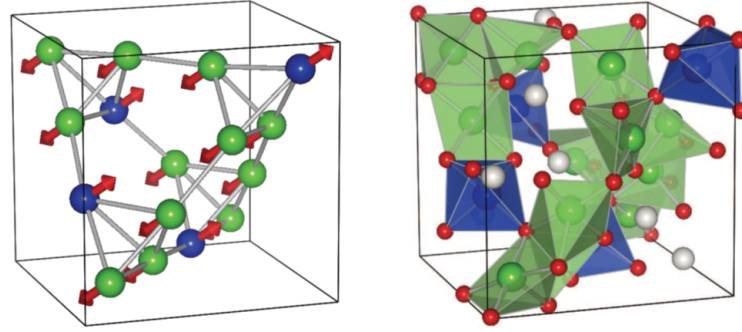
Figure 1.2 – Crystal structure of Cu_2OSeO_3, characterized by two inequivalent Cu^{2+} sites with different oxygen coordination. Representing 3 up 1 down type ferrimagnetic spin alignment [1]

Skyrmion phase. Also, the application of small (250 Oe) magnetic field, away from the critical temperature, leads to formation of conical phase.

Now we talk about the magnetoelectric coupling in the Cu_2OSeO_3. For the given spin texture $\vec{m}(\vec{r})$, the polarization $\vec{P}$ and $\vec{M}$ are predicted by d-p hybridization scheme as follows [12]

$$\vec{P} \propto \frac{1}{\int d\vec{r}} \int \sum_{i,j} [\vec{e}_{ij}.\vec{m}(\vec{r})]^2 \vec{e}_{ij} d\vec{r} \qquad (1.1)$$

$$\vec{M} \propto \frac{\int \vec{m}(\vec{r}) d\vec{r}}{\int d\vec{r}} \qquad (1.2)$$

Summation has been taken over 80 Cu-O bonds within one crystallographic unit cell whereas integral is taken over one magnetic unit cell. Size of magnetic unit cell is larger than crystallographic unit cell. Thus we can assume collinear state for one crystallographic unit cell.

For the helical phase, Spin texture can be described as

$$\vec{m}(\vec{r}) \propto \vec{e}_z M_1 + [\vec{e}_x cos(\vec{q}.\vec{r}) + sin(\vec{q}.\vec{r})], \qquad (1.3)$$

where $\vec{e}_x$, $\vec{e}_y$, $\vec{e}_z$ are unit vectors perpendicular to each other and $\vec{e}_z$ and $\vec{q}$ are parallel to applied magnetic field.

For the Skyrmion phase, magnetic spin texture can be defined as

$$\vec{m}(\vec{r}) \propto \vec{e}_z M_2 + \sum_{a=1}^{3} [\vec{e}_z cos(\vec{q}_a.\vec{r} + \Pi) + \vec{e}_a sin(\vec{q}_a.\vec{r} + \Pi)], \qquad (1.4)$$

Where $\vec{q}_a$ denotes one of the three magnetic modulation vectors normal to applied magnetic field. $\vec{q}_a$ form the angle of deg 120 with each other. $\vec{e}_a$ is unit vector orthogonal to $\vec{e}_z$ and $\vec{q}_a$ defined using left handed system or right handed system, so as to have consistency in signs.

M_1 and M_2 are found by normalizing the spin density.

Now I will show the simulations for polarization induced by magnetic field applied in different directions on Cu_2OSeO_3, in skyrmion phase, in fig 1.4-fig 1.6 . These simulations are for illustration and understanding purpose and match with the results given in the paper by S.Seki et al [12].

For simulation purpose, the periodicity of magnetic unit cell of Skyrmions was taken as 70nm.

Further I calculated the polarization component along the magnetic field for different orientations of magnetic field. The simulation is shown in the figure 1.7.

More theoretical and experimental details about the magnetic skyrmions can be found in [2, 13–16].

I conclude this chapter by showing some important materials,in fig 1.8, in which skyrmions have been observed.
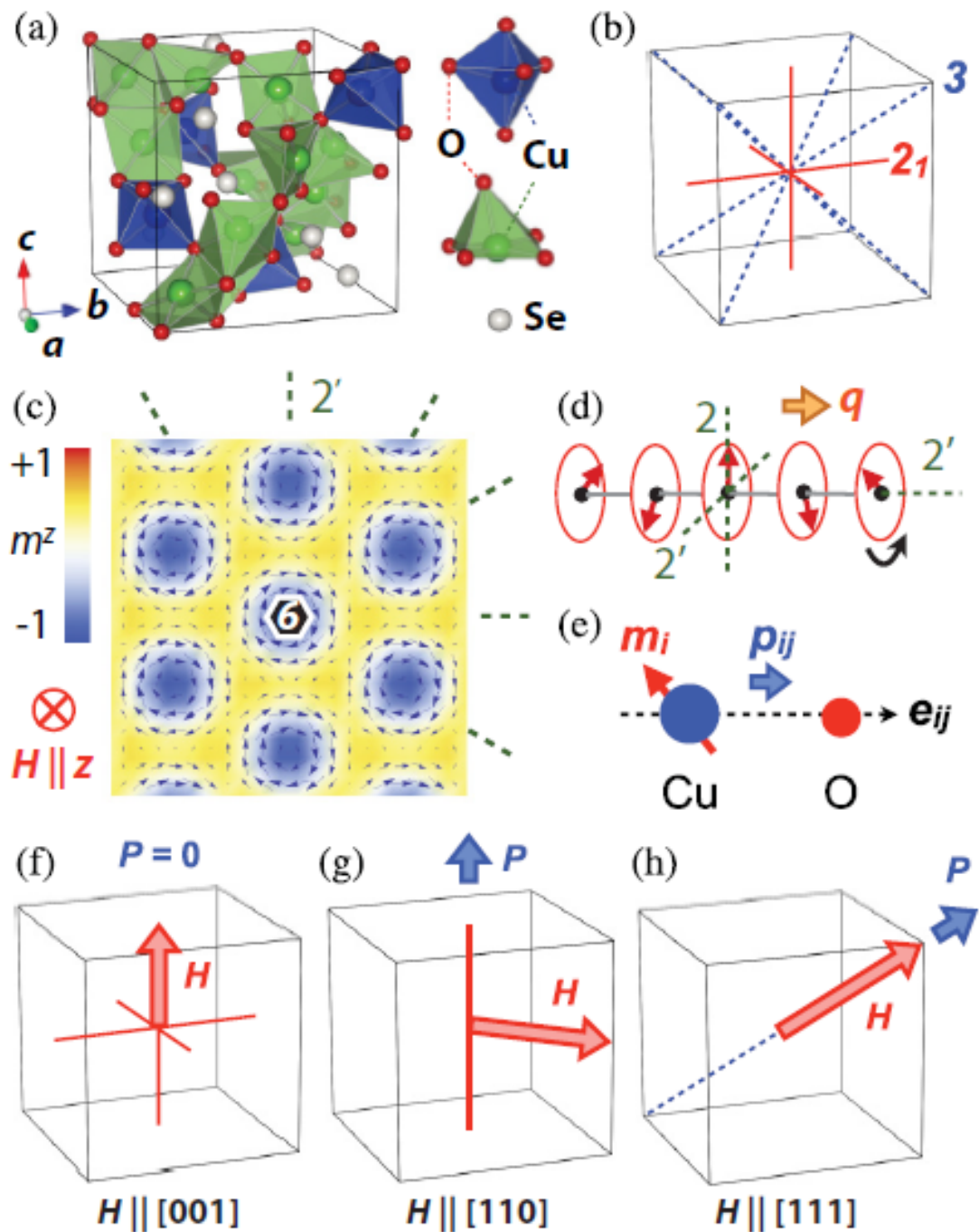
Figure 1.3 – a: Crystal structure of Cu_2OSeO_3
b: Symmetry elements compatible with the crystal lattice of Cu_2OSeO_3
c: Magnetic skyrmion crystal formed within a plane normal to applied magnetic field (H).
Background color represents the out-of-plane component of local magnetization vector ($\vec{m}_z$).
d: Proper screw helical spin texture with a magnetic modulation vector q. Here, green dashed
lines represent two fold rotation axes or two-fold rotation axes followed by time reversal, and
a small black hexagon does a six fold rotation axis along the out-of-plane direction.
e:Schematic illustration of d-p hybridization mechanism.
f-h: Magnetically induced electric polarization P under various directions of H for Cu_2OSeO_3
[12]
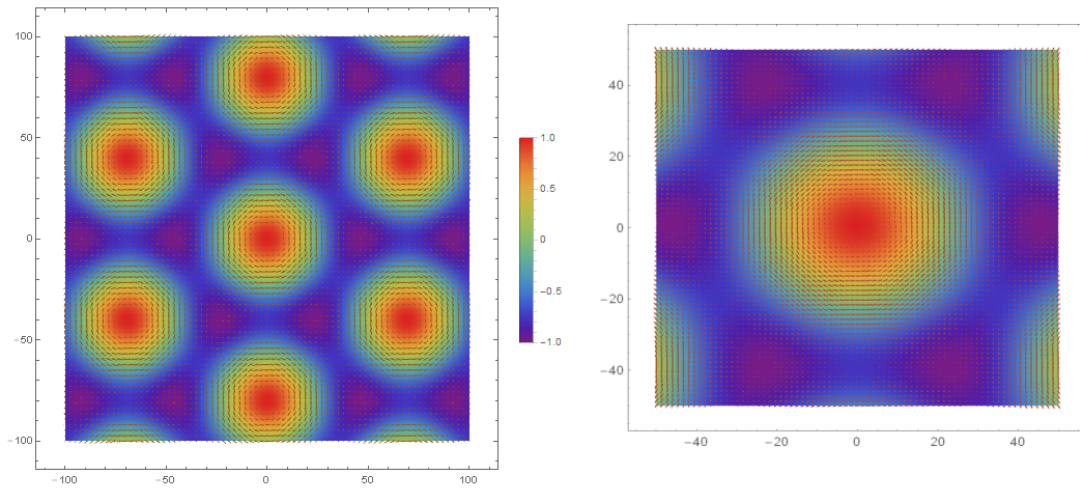
Figure 1.4 – Calculated spatial distribution of local magnetization vector $\vec{m}(\vec{r})$, Axes represent the plane perpendicular to which, magnetic field has been applied. Colorbar represents the normalized values of local magnetization vector
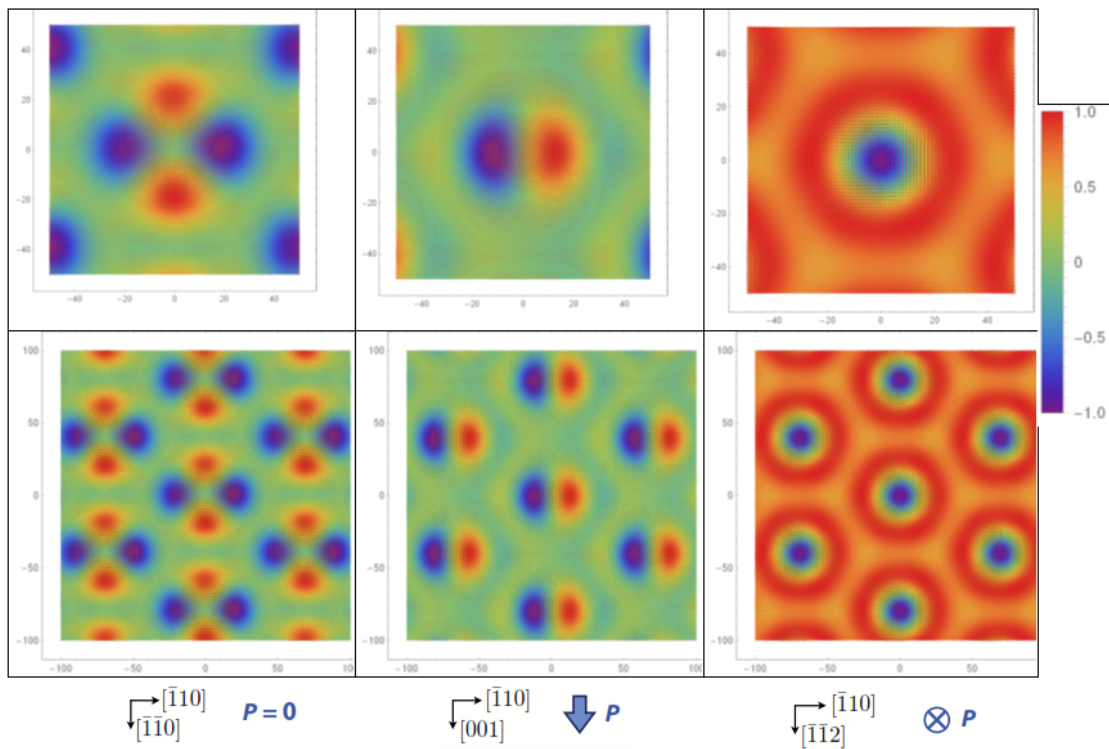
Figure 1.5 – Calculated spatial distribution of local polarization vector with different orientations of magnetic field. Figures in the first row represent single magnetic unit cells. Figures in second row contain multiple magnetic unit cells. Axes represent the plane perpendicular to which, magnetic field has been applied. Colorbar represents the normalized values of local polarization vector
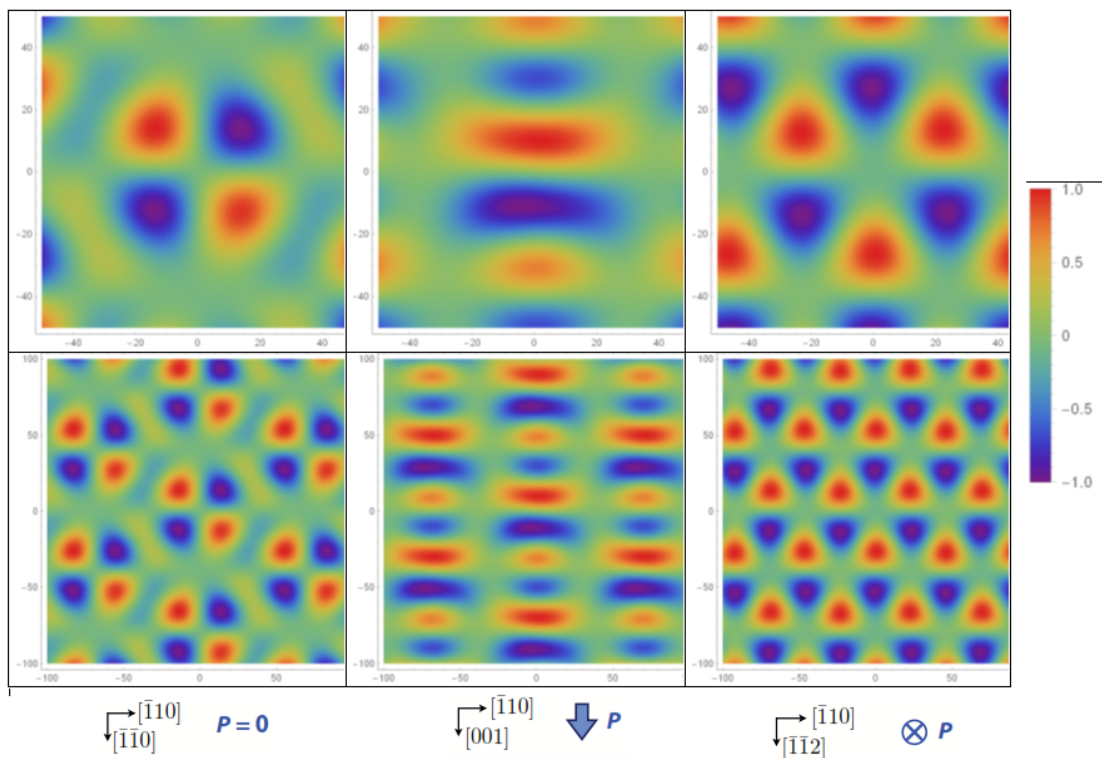
Figure 1.6 – Calculated spatial distribution of local electric charge with different orientations of magnetic field.Figures in the first row represent single magnetic unit cells. Figures in second row contain multiple magnetic unit cells.Axes represent the plane perpendicular to which, magnetic field has been applied. Colorbar represents the normalized values of local electric
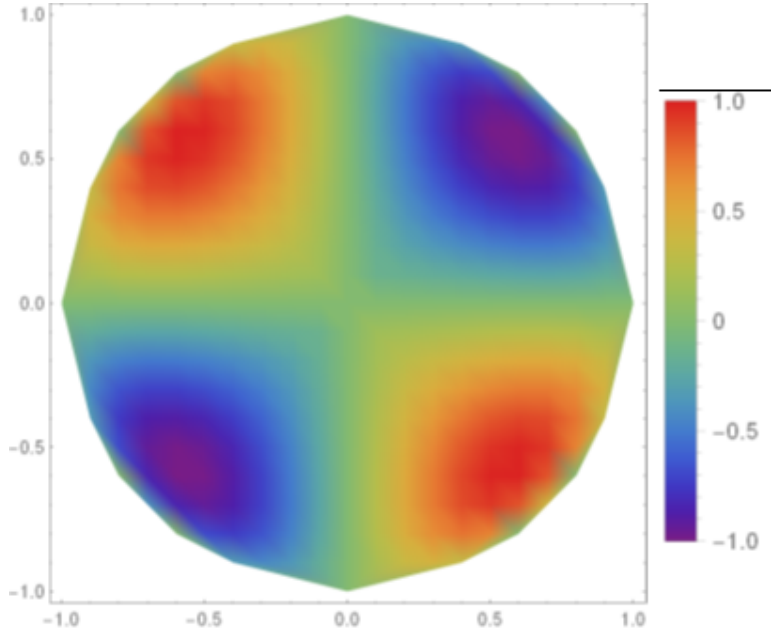
Figure 1.7 – Variation of polarization component along the applied field with orientation of magnetic field.The axes represent the normalized planes perpendicular to which magnetic field has been applied. We see that, for magnetic field along [111] (represented by $[\frac{1}{\sqrt{3}} \frac{1}{\sqrt{3}} \frac{1}{\sqrt{3}}]$ in this figure) or $[\bar{1}\bar{1}\bar{1}]$, the polarization is always induced in [111] direction.

| Category	Material	T_c (K)	λ_m (nm)	Conductivity
Chiral-lattice ferromagnets	MnSi	30	18	Metal
	$Fe_{1-x}Co_xSi$	<36	$40 \sim 230$	Semiconductor
	MnGe	170	3	Metal
	FeGe	278	70	Metal
	Cu_2OSeO_3	59	62	Insulator
Centrosymmetric ferromagnets	$Y_3Fe_5O_{12}$	560	>500	Insulator
	$RFeO_3$	>600	>100,000	Insulator
	$BaFe_{11.79}Sc_{0.16}Mg_{0.05}O_{19}$	>300	200	Insulator
	$La_{1.37}Sr_{1.63}Mn_2O_7$	100	160	Insulator
Interface	Fe/Ir(111)	(>300)	1	Metal
	FePd/Ir(111)	(>300)	7	Metal

Figure 1.8 – List of materials hosting skyrmion spin texture. Magnetic ordering temperature T_c and spin modulation period λ_m are also indicated [2]

2 Experimental Techniques

2.1 Introduction

Different types of techniques have been used to observe different kind of phase transitions. Sensitivity of particular technique depends on the phenomenon being studied. Some technique may be suitable for studying for one kind of phase transitions while not for other. For studying thermodynamics of phase transitions, specific heat measurements can also be used. To study phase transitions in magnetic materials, magnetometry measurements are widely used. Neutron scattering experiments may also be used to observe the different kind of phases in the materials [11]. Lorentz Transmission Electron microscopy experiments may also be useful to give real time dynamics of the spin structures under various external forces [17]. Considering the cost and effort involved in the neutron scattering experiments and electron microscopy experiments, magnetometry measurements seem to be more suitable for magnetic materials, if we have to study the systems under equilibrium or quasi-static states. In magnetometry measurements,the most basic measurements are the magnetization measurements. Magnetization measurements are not particularly sensitive to phase transitions. Thus more sensitive techniques like AC magnetic susceptibility are used to determine the phase transitions. In the context of studying phase transitions in Cu_2OSeO_3, it has been shown by Omrani et al. [7, 8] that magnetoelectric susceptibility technique is more sensitive than the widely used AC magnetic susceptibility technique. The reason for this sensitivity is the magnetoelectric coupling observed in this material which can be used as a parameter to study phase transitions in more effective way. In the present chapter, I will describe magnetization measurements shortly and then I will go on to describe the theoretical framework of magnetoelectric susceptibility measurements.

2.1.1 Magnetization measurements

Magnetization is measured by the SQUID sensor which is calibrated to give voltage signal corresponding to the magnetic moment using standard NIST YIG sample. To determine the different magnetic orderings, we perform magnetic field scan or temperature scan (i.e measure

magnetization of the sample in particular orientation (in case of single crystal) with variation of applied magnetic field or temperature).

2.1.2 Magnetoelectric susceptibility

For the compounds, showing magnetoelectric coupling i.e interaction between magnetic ordering and electric ordering parameters,the measure of the magnetization in response to applied AC electric field of particular frequency and amplitude is a sensitive and faster method for determining phase boundaries. In the perspective of current thesis, to study the single crystals of Cu_2OSeO_3 (which shows magnetoelectric coupling), this technique has been used extensively.

Meaning of Magnetoelectric Susceptibility response

Suppose we are giving the AC electric field to the sample, which can be written as,

$$E = E_0 sin\omega t \tag{2.1}$$

which will generate the Squid response V(E), which can be expanded as

$$V(E) = V(0) + \frac{dV(0)}{dE}E + \frac{1}{2}\frac{d^2V(0)}{dE^2}E^2 \tag{2.2}$$

Since Squid response is directly proportional to the magnetization in the sample, magnetization can be written as

$$M(E) = M(0) + \frac{dM}{dE}\Big|_{E=0}E + \frac{1}{2}\frac{d^2M}{dE^2}\Big|_{E=0}E^2 \tag{2.3}$$

or upto first order

$$M(E) = M(0) + \frac{dM}{dE}\Big|_{E=0}E_0 sin\omega t + O(sin2\omega t, ----) \tag{2.4}$$

The term $\frac{dM}{dE}\Big|_{E=0}$ is called the magnetoelectric susceptibility term. Now suppose we also apply a constant DC electric field E_1 across the sample. Then we can expand the Squid response and hence the magnetization response of the sample around E_1. Thus we will be looking at the term $\frac{dM}{dE}\Big|_{E=E_1}$ for the applied DC field E_1. Units used to represent this term are generally emu/(V/mm), $emu/(V/\mu m)$ or $\mu_B/(V/\mu m)$.

From this definition of magnetoelectric susceptibility, as the coefficient of the magnetization term oscillating at excitation frequency, it is clear that this can be measured easily using Lock-

In amplifier which can be locked at particular frequency and phase, thus eliminating other higher harmonics. Further, it is not necessary that magnetization response should exactly follow the excitation signal. It may lag behind the signal that means there will be phase mismatch. This will give rise to Imaginary component of the magnetoelectric susceptibility signal. This phase lag actually represents the dissipative or absorption processes inside the material which act like resistance for the spin configuration to change according to external stimuli. Magnetic field can couple with the magnetic structure of the material directly whereas electric field needs to be coupled with the magnetic order parameters for affecting the magnetization response. Thus materials having magnetolectric coupling can produce magnetization on application of electric field or polarization on application of magnetic field. Another thing to note is that, magnetoelectric susceptibility technique is applicable to those compounds in which there is magnetoelectric coupling. If there is no polarization at particular magnetic field, magnetoelectric susceptibility should also go to zero at that point. Though magnetoelectric suscetibility may also go to zero if the polarization is constant with the application of field as is the case in the polarized/ ferrimagnetic phase.

2.1.3   Comparison of sensitivity with other techniques

Omrani et. al [7, 8] have made the comparative study of different techniques for studying the phase transitions in Cu_2OSeO_3. The figure 2.1 shows that magnetoelectric susceptibility is more sensitive to phase boundaries compared to magnetization measurements or AC magnetic susceptibility.

2.1.4   Phase correction procedure for Magnetoelectric Susceptibility

Because of passive components in the circuit, the actual response is combination of sample response and instrument phase. We can perform the phase correction later by multiplying the real and imaginary components to a rotation matrix. The phase is chosen such that the imaginary component should go to zero in polarized phase. This is done as follows

$$\begin{bmatrix} R1 \\ I1 \end{bmatrix} = \begin{bmatrix} cos\theta & -sin\theta \\ sin\theta & cos\theta \end{bmatrix} \begin{bmatrix} R \\ I \end{bmatrix},$$

where $\begin{bmatrix} R1 \\ I1 \end{bmatrix}$ represents phase corrected real and Imaginary parts of dM/dE signal. θ is the phase which is due to instrument response.

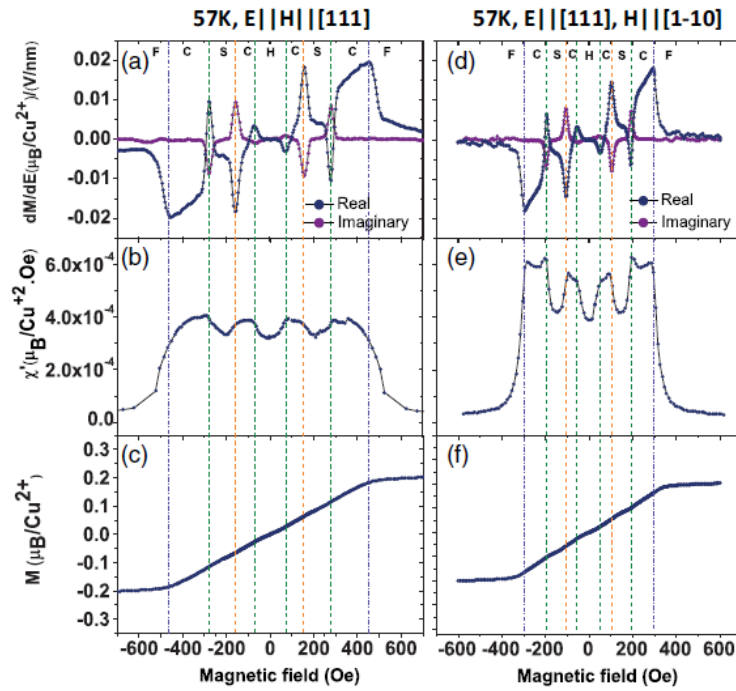More details about theory of magnetoelectric susceptibility can be found in [7, 18].

Figure 2.1 – The magnetic field dependence of:

a,d: AC ME susceptibility

b,e: AC magnetic susceptibility

c,f: DC magnetization for $E||\mu_0 H||[111]$ in a to c and $E||\mu_0[111]$, $\mu_0 H||[1-10]$,The letters F, C, S, and H denote the ferrimagnetic, conical, skyrmion, and helical phases, respectively, [7]

3 Experimental Setup

In this chapter, I will describe the experimental setup used for performing the Magnetisation and Magnetolelectric Susceptibility measurements. Thereafter, I will describe different measurements performed.

3.1   Experimental Setup

Low temperature Measurements were performed at Cryogenic-SQUID setup S700X , the schematic of which is shown in fig 3.1.
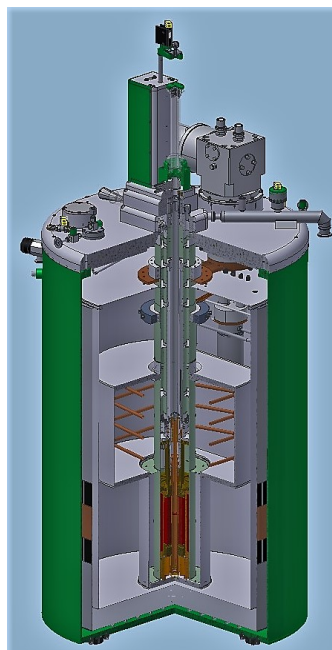

Figure 3.1 – Cryostat setup including VTI(Variable Temperature Insert) for Low temperature measurements down to Liquid Helium Temperature (from Cryogenic Squid S700X manual)
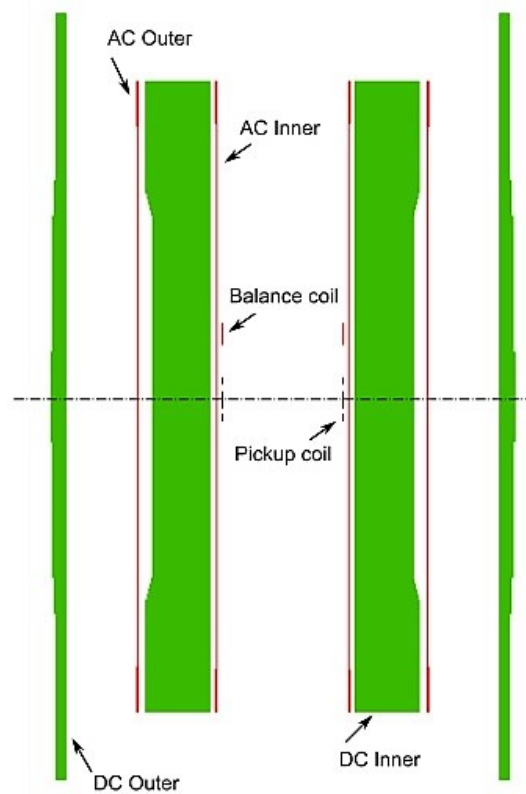
Figure 3.2 – Schematic of superconducting magnet coil assembly(from Cryogenic Squid S700X manual)

3.1.1 Magnetic Field in the setup

Magnetic field in the system is generated using a superconducting magnet which generates homogeneous magnetic field upto 7T in 4cm vertical region of magnet centre. The schematic of magnet is shown in fig 3.2 .In the experiments, magnetic field has been used in the persistent mode (i.e.once reached to desired constant value, it remains there without need for external power supply, because of closed superconducting loop). This provides more stable magnetic field than in the hysteresis mode

3.1.2 Temperature control in the setup

The inside of VTI(Variable Temperature Insert) is insulated to helium reservoir through vacuum. Liquid helium flow occurs to the VTI through the needle valve from helium reservoir The impedance of valve causes the sudden pressure drop which leads to cooling (down to 1.5K) and vaporization of liquid Helium by Joule Thomson effect. Cooled gas passes through heat exchanger and heated to the set temperature before it enters into sample chamber. There is another auxiliary heater near the sample chamber to improve the heating rates.

There are two thermometers for the temperature measurement. Thermometer A, located on the heat exchanger measures the temperature of the heated gas. Thermometer B, located above the sample chamber, measures effectively the temperature of sample at equilibrium condition.

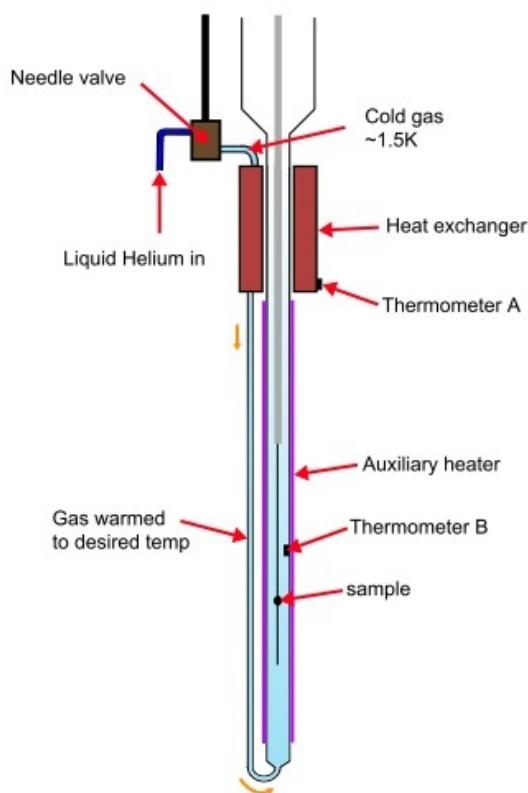Schematic of temperature control is shown in fig 3.3.

Figure 3.3 – Schematic view of temperature control in S700X Squid setup(from Cryogenic Squid S700X manual)

3.2 Design of new sample probe for magnetoelectric susceptibility measurements

The main aim for designing the new sample probe was to achieve the high electric field even for the thick samples.

3.2.1 Design of sample holder

The sample holder was designed to apply the high uniform electric field on the sample. The sample holder was made using the standard PCB(Printed Circuit Board) material FR-4 of 0.8

mm thickness, with the 35 um coating of copper layer for making the one side electric contact with the sample (Thus using two such pieces with the sample glued between them). To place the sample in plane perpendicular to magnetic field, as much as possible, the corners of the sample holder were grooved, so as to place it straight with the help of two thin sticks of PCB material FR-4. These two PCB sticks are also having the 35 um thick coating of copper layer for carrying the voltage from the source coupled with the AC excitation signal for measurement. The corner space (0.5mm) of the sample holder and of the PCB sticks was not coated with copper layer, so as to avoid any unwanted electric contact. Besides the aim to apply the high voltage, this sample holder would also work as the support for polishing the samples down to micrometer thickness. I made the design of sample holder on ORCAD PCB designer and it was manufactured by workshop at EPFL.

The image of final design of sample holder and PCB sticks are shown in fig 3.4 and fig 3.7.
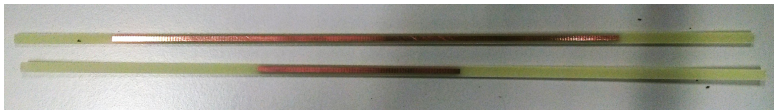

Figure 3.4 – Design of PCB sticks

The PCB designs can be seen in fig A.1 in appendix.

3.2.2 Design of upper detachable part of the sample probe

For giving the voltage supply from the source to the sample, we needed the connector mounted on the sample probe. With the high voltage application in mind, it was necessary the connector should be put inside a casing of insulator material which will be mounted on the steel probe. For this purpose, delrin was used. The design also included the O-rings to make the assembly air-sealed. The upper assembly is completed detachable from the remaining part so that it can be removed if the sample probe needs to be taken out from the airlock.

The 3-D design and 2-D schematic of different parts can be seen in fig A.2 in appendix.
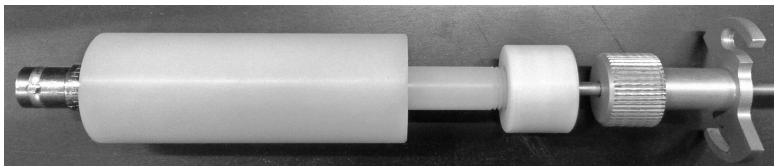
The full upper assembly is shown in fig.3.5

Figure 3.5 – Upper part Assembly

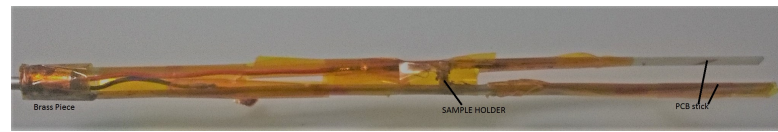The full lower assembly for holding the sample inide VTI is shown in fig.3.6

Figure 3.6 – Full Lower assemply attached with sample probe

3.2.3 Design of brass piece

Brass pieces were designed to be put on the sample probe to hold the PCB sticks by glueing either by varnish or by STYCAST. Brass is used because it is non-magnetic and will not give any spurious signal. 3-D design and 2-D schematic can be seen in fig A-7 and fig A-8 in appendix. Image of brass piece is shown in fig. 3.7.
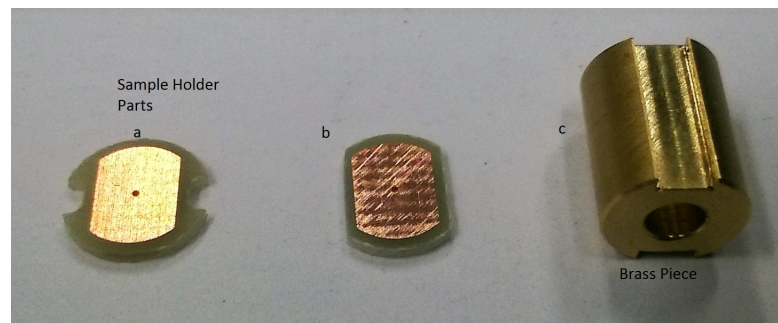

Figure 3.7 – Design of two parts of sample holder and brass piece

3.3 AC+DC coupler

In magnetoelectric susceptibility (dM/dE) measurements, excitation signal is given by internal oscillator of the Lock-In amplifier and squid response is recorded by Lock-In amplifier locked at its internal frequency.Lock-In amplifier is locked with zero phase. Further, if we have to provide the DC bias to the sample, as is the main intention of this thesis, we have to couple the DC and AC signals. The AC and DC signals can't be combined directly efficiently because of mutual feedbacks causing the spurious signals (not sinusoidal with DC bias). We had the Lock-In amplifier which can provide the AC signal and DC signal of 10 V (+ or -). We had another voltage amplifier, which could amplify the input signal from Lock-In amplifier and provide output signal in the range of 2 KV (+ or -). So we thought of coupling the DC and AC signal and then provide it to amplifier. In any case, it is always better to couple the signals first and then amplify. It would be difficult to couple the signals after amplification because the capacitors and inductors in the coupler circuit must be able to sustain that much voltage, which is not a good practice. Thus we made the coupler to couple AC and DC signals at low voltage side and then amplified it through amplifier. The schematic of the AC+ DC coupler is shown in fig 3.8:
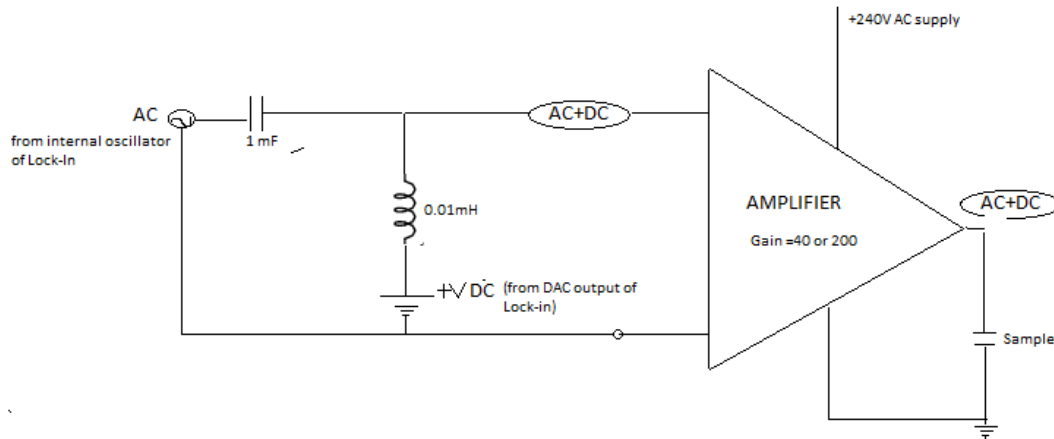
Figure 3.8 – Schematic of simple LC circuit for coupling AC and DC signal and amplifier to amplify the mixed signal

3.4 Sample preparation

The single crystals of Copper Oxo Selenite (Cu_2OSeO_3) were grown by standard chemical vapour transport method by Dr. Arnaud Magrez at EPFL as given in ref[5]. Then, I aligned single crystal of Cu_2OSeO_3 along [111] direction using Laue diffraction pattern and cut the crystal using wire saw. Then crystals were polished down to desired thickness. The figure 3.9 shows the image of the polished sample glued on the substrate with GM varnish.

Figure 3.9 – Picture of Polished sample glued on the substrate with [111] direction perpendicular to the substrate plane

Figure 3.10 – Laue diffraction pattern for [111] orientation of the sample.The pattern with red circles is the simulated pattern to compare

There have been two samples used in the experiment. The thickness of samples were 620 um and 50 um along [111] direction and the mass of the samples were 0.0212 g and 0.005 g respectively. The surface dimensions perpendicular to [111] direction were approximately 2 mm× 1.5 mm and 3.5 mm × 2.5 mm respectively.

The Laue diffraction pattern for [111] direction is shown in fig 3.10.

4 Magnetization and Magnetoelectric Susceptibility Measurements

4.1 Calibration

Squid sensor needs to be calibrated first time using the standard NIST sample of YIG (Yttrium Iron Garnet), which is a magnetic moment standard, at the 298 K with range of magnetic fields. The calibrated value for the squid sensor in range 1 was found to be 2.344 emu/V.

4.2 Magnetization measurements on 0.62 mm samples

The main purpose of these measurements is to check the saturation magnetization of the sample and also to compare the sensitiveness of our technique(magnetoelectric susceptibility) with other techniques.

Magnetization measurements were performed for 0.62 mm thick sample. The magnetic field was applied along the direction of [111] of the crystal and magnetization was measured using the squid sensor.

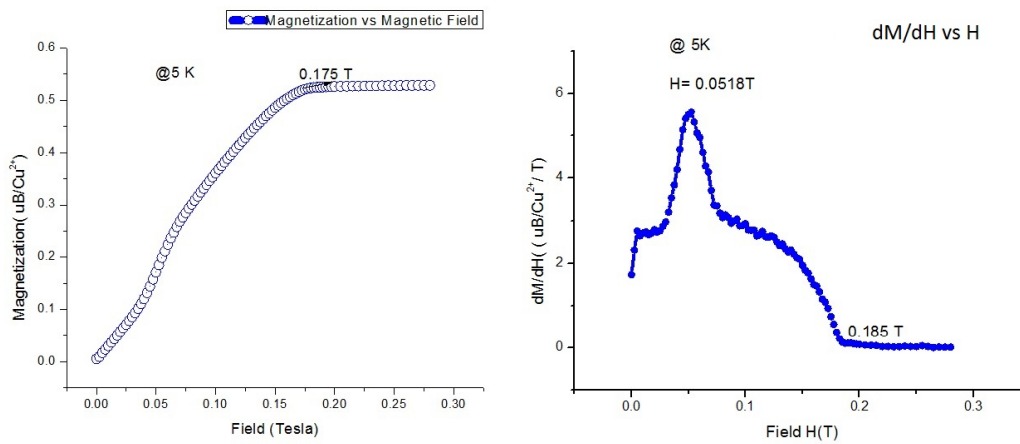The magnetization curves (field scans) at 5K and 58.1 K are shown in fig 4.1 and fig 4.2:

Figure 4.1 – Magnetization vs magnetic field (M-H) curve at 5K for the magnetic field applied along [111] direction. At high fields, magnetization tends to 0.5 $\mu B/Cu^{2+}$ which is the expected saturation magnetization at 0 K for this sample
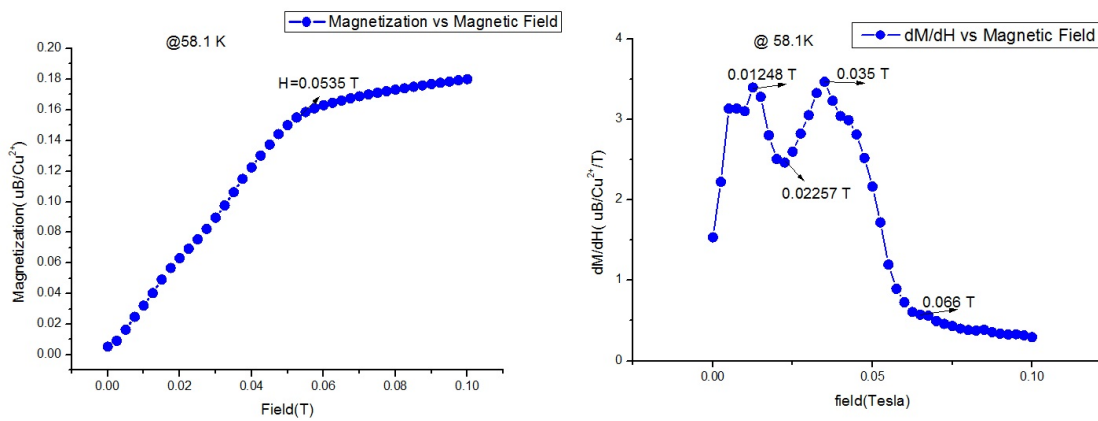

Figure 4.2 – Magnetization vs Magnetic Field (M-H) curve at 58 K for the magnetic field applied along [111] direction. At high fields, magnetization tends to 0.18 $\mu B/Cu^{2+}$

The dM/dH curves along side the magnetisation curves are the mathematical derivatives.

From the magnetisation curve at 5 K, we can observe that saturation magnetization of the sample is near 0.5 Bohr magneton per copper site. From the crystal structure of Cu_2OSeO_3, we can see that spin configuration in the lattice is 3 up -1 down. That gives the average magnetisation value of 0.5 bohr magneton per copper site in the lattice at absolute temperature(0 K).Thus magnetic behaviour of the sample is as per the expectation. Further we observe the lower saturation magnetization for the 58.1 K . This is expected because magnetization in the lattice has the temperature dependence as do the other magnetic materials such as iron, copper, nickel(but not necessarily in same way).

From the field scans of magnetization at 5K or 58.1K, we observe that there is only one

prominent feature clearly visible, the onset of ferrimagnetic phase from conical phase. There is one small feature at 0.05 T in field scan at 5K but not visible clearly in field scan of 58.1K . The mathematical derivative (i.e.dM/dH) curves show these features more clearly. Thus we observe helical to conical phase transition at 518 Oe at 5K. For the field scan at 58.1 K, it is difficult to quantify the boundaries for various phase transitions. The temperature scans were also performed for 160 Oe and 200 Oe fields after cooling in magnetic field and after zero field cooling. The curves are shown in fig 4.3 and fig 4.4.
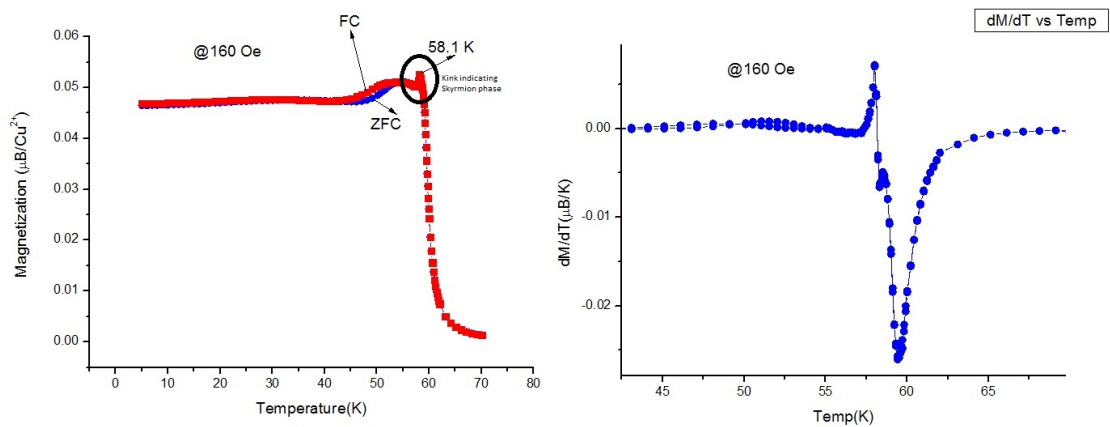
Figure 4.3 – Temperature scans of magnetization at 160 Oe, while cooling with magnetic field (FC) and while doing zero field cooling (ZFC)
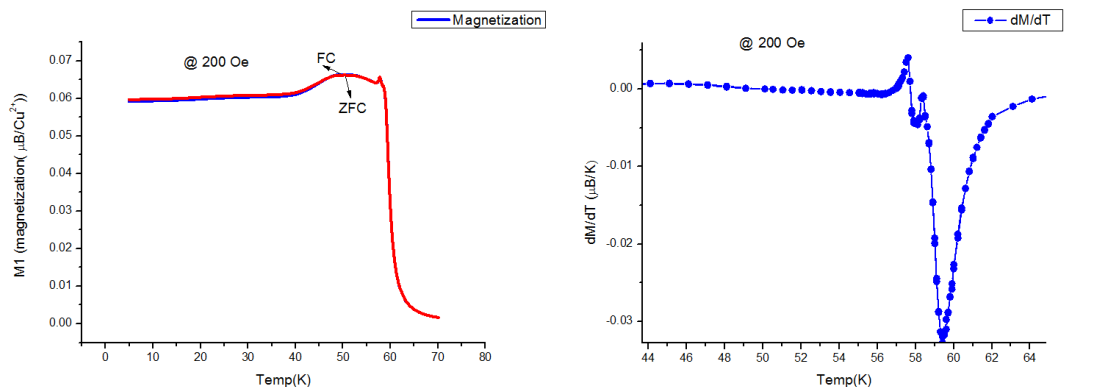

Figure 4.4 – Temperature scans of magnetization at 200 Oe, while cooling with magnetic field (FC) and while doing zero field cooling (ZFC)
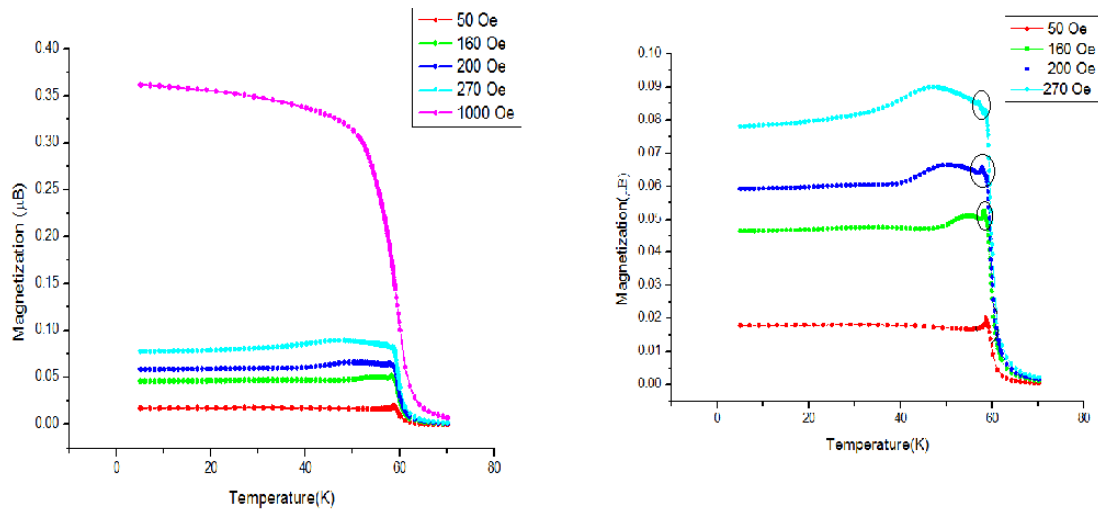
Figure 4.5 – Temperature scan of magetization at different magnetic fields for determining the features representing Skyrmion phase. The small first kink (circled) at 160-270 Oe is the signature of skyrmion phase. If seen properly there is another sharp transition after the kink. It is paramagnetic phase transition. In case of 50 Oe, only one transition, the paramagnetic transition is visible
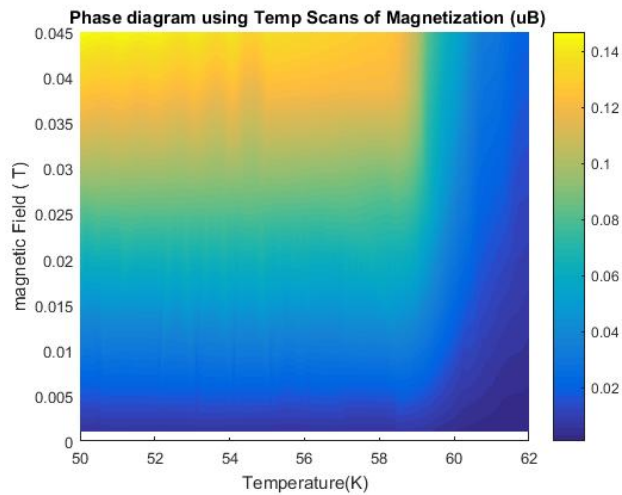

Figure 4.6 – Phase diagram for temperature scans of magnetizations at different magnetic field. There is no contrast for determining skyrmion phase boundary

The skyrmion phase in these curves is characterized by small kink at 58.1 K as shown in fig 4.3 by circular mark. We can see that difference between FC and ZFC curves is large at 160 Oe in compared to 200Oe. Also there is no observable difference in magnetization in Skyrmion phase for FC and ZFC curves. It can be seen, in fig 4.5, that there is no kink for the temperature

scan at 1000 Oe because there is no Skyrmion phase observed at this field. The phase digram for magnetization curve is shown in fig 4.6. Because of very small peak representing Skyrmion boundary , skyrmion boundary is not sharp .

Further, I calculated the mathematical derivatives dM/dT from these temperature scans. The dM/dT curves are shown in fig 4.7. There are some more phase transition features visible from these dM/dT curves. The large negative peak represents the transition from ordered phase to paramagnetic phase. The peak near to negative peak represent the upper boundary of skyrmion phase and lower temperature peak represents lower boundary of Skyrmion phase. Though helical to conical phase boundary is not visible.This is more clear from the phase diagram shown in fig 4.8.
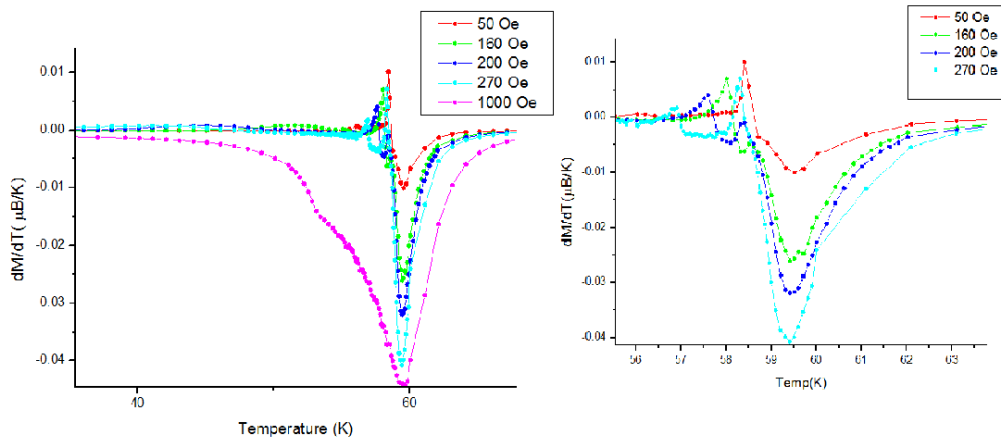

Figure 4.7 – dM/dT curves using mathematical derivative. These curves show some peaks which can be related to Skyrmion phase.
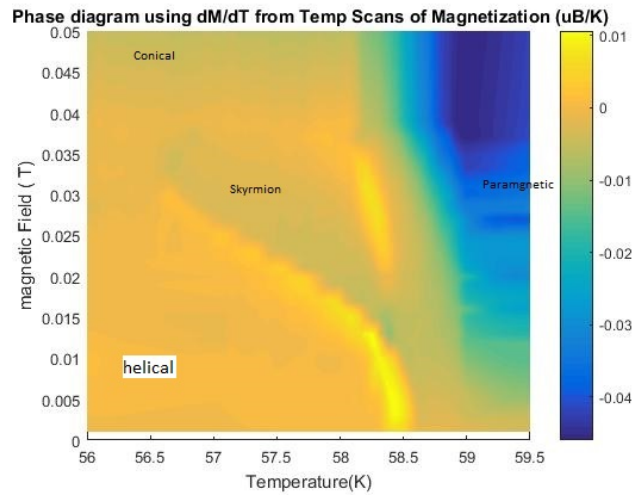
Figure 4.8 – Phase diagrams from calculated dM/dT. These diagrams show better contrast for Skyrmion phase boundary. Though helical to conical phase boundary is not visible

From the phase digram in fig 4.8, the skyrmion phase boundary is visible but contrast is still not that good.

4.3 Magnetoelectric susceptibiltiy(dM/dE) measurements with zero dc electric field on 0.62 mm sample

dM/dE measurements are performed and real and imaginary part of dM/dE are phase corrected (rotation by particular angle) assuming that imaginary part should completely go to zero near upper boundary(skyrmion to conical) of skyrmion phase. The phase correction was found to be 0.278 radians. This is a constant (as it should be), independent of field, temperature. It only depend on instrument parameters.Thus for same set-up and sample, this will remain same. It has been observed that magnetoelectric susceptibility technique works well only in the low-frequency regime. The reason for this behaviour is not known. This might be related to very high relaxation times (in order of milliseconds) at the phase boundaries. For our experimental purpose, **8.3Hz** was chosen as the excitation frequency. In all the dM/DE measurements, we have applied field along [111] direction and measured the response also along [111].

4.3.1 Magnetic field scans

Field scans for dM/dE were performed to understand and compare the features representing the phase transitions.

Field scans at 57.6K for real part and imaginary part of magnetoelectric susceptibility signal before and after phase correction are shown in fig 4.9 and fig 4.10 .
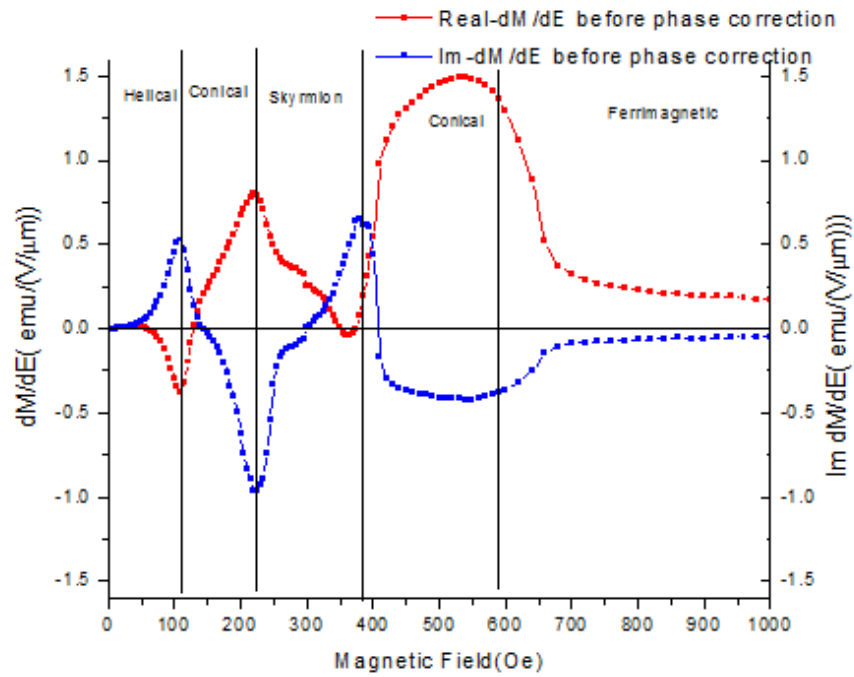
Figure 4.9 – dMdE signal, field scan at 57.6K before doing phase correction. In this case, due to mixing of instrument response, imaginary part of the signal is non-zero in polarized/ferrimagnetic phase
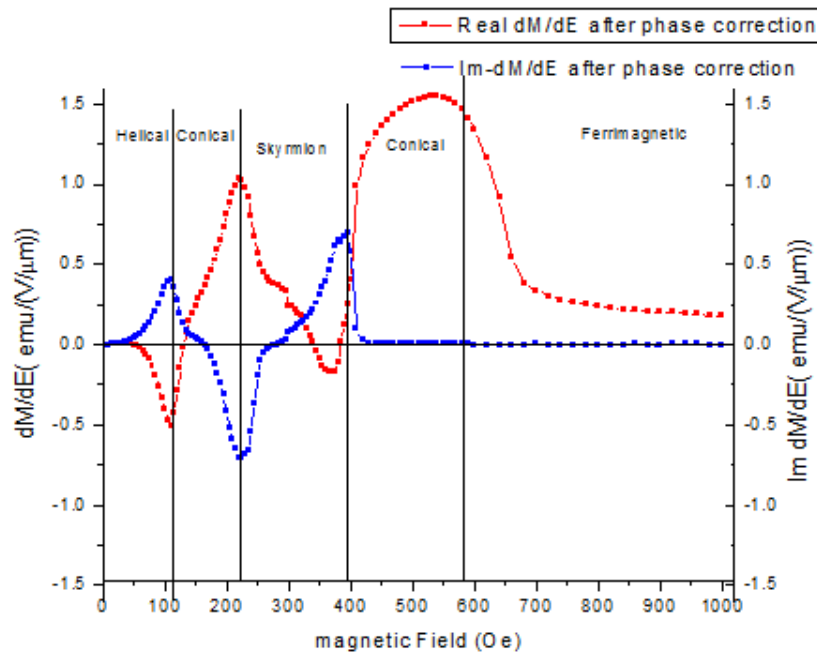

Figure 4.10 – dM/dE signal, Field scan after phase correction. Now imaginary component of dM/dE signal goes to zero in polarized phase

There is no change in shape of curves except that imaginary component being zero in ferrimagnetic phase after phase correction. We identify the peaks and corresponding phase transitions as given in [7]. We can clearly observe peaks in dM/dE signal at the phase boundaries between helical to conical phase, conical to Skyrmion phase, Skyrmion to conical phase and conical to ferrimagnetic phase. Further, dM/dE signal going to zero, inside any ordered phase, may correspond to two types of features. Either the polarization at particular point is zero thus there is no magnetoelectric response; or polarization is constant with applied magnetic field which will also lead to zero magnetoelectric response which should be the case in polarized/ferri phase when magnetization and polarization are saturated. But we observe small signal in the polarized phase.

Field scans for real and imaginary part of dM/dE signal at different temperatures are shown in fig 4.11 and fig 4.12.
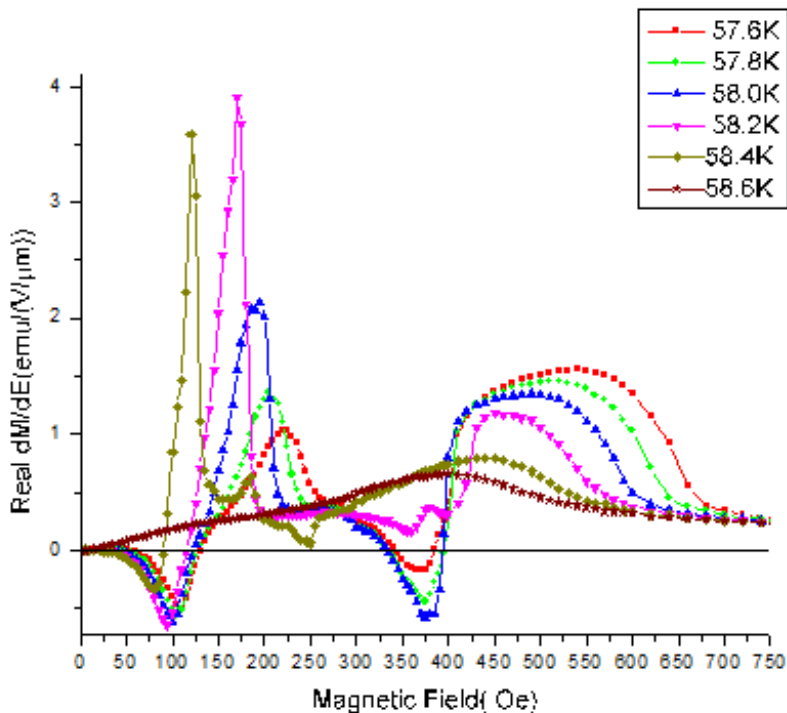

Figure 4.11 – Field scans for 0.62 mm sample at different temperatures for magnetic field along [111] direction and response also being measured along [111] direction. The excitation frequency is 8.3Hz

4.3. Magnetoelectric susceptibiltiy(dM/dE) measurements with zero dc electric field on 0.62 mm sample
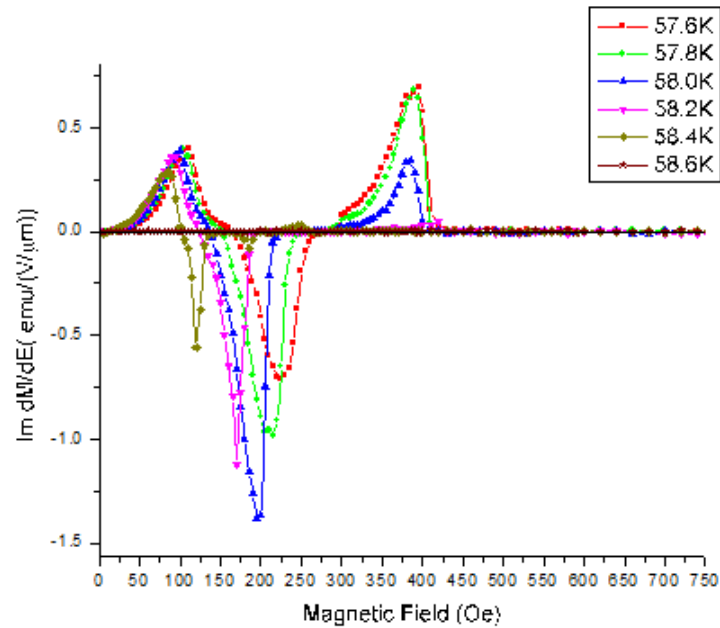

Figure 4.12 – Field scans showing Imaginary part of ME response for 0.62 mm sample at different temperatures for magnetic field along [111] direction and response also being measured along [111] direction. The excitation frequency is 8.3Hz. These scans are presented after phase correction procedure

From these figures, we can see that lower skyrmion boundary shifts (in magnetic field) much more rapidly with temperature than other phase boundaries. That means conical to skyrmion phase transition is very much sensitive to temperature-field conditions.

Further temperature scans were performed at different fields.

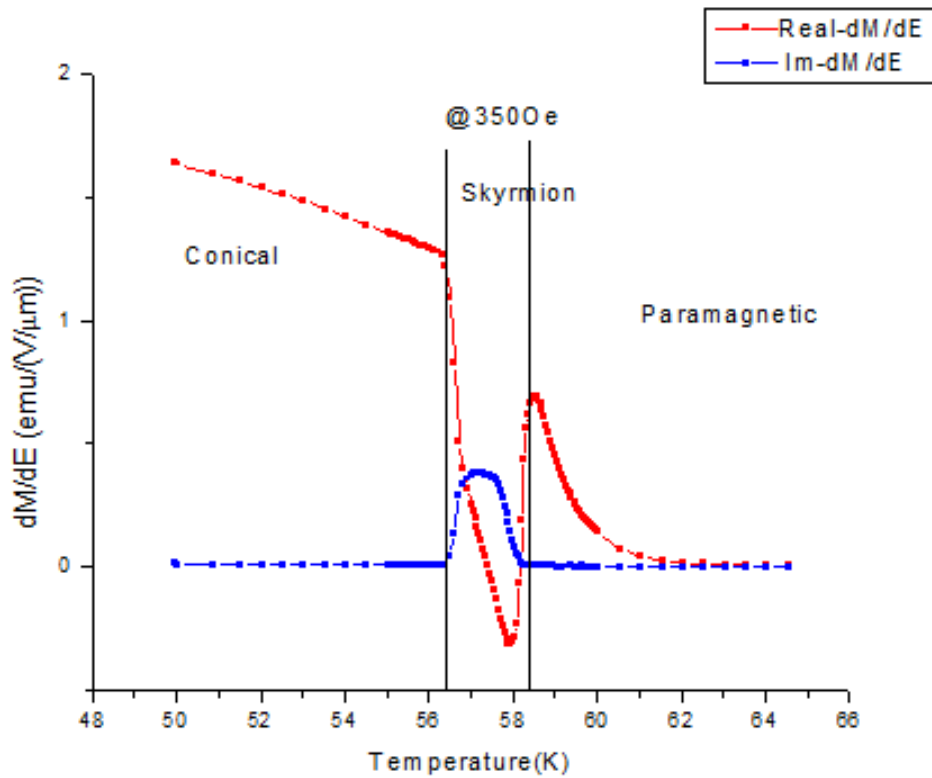First I show the feature representing the Skyrmion phase in temperature scan in fig 4.13.

Figure 4.13 – Temperature scan showing a dip representing the skyrmion state

We see,in fig 4.13, that Skyrmion phase is recognized by a dip or broad peak in real or imaginary part of temperature scans. This is in contrast to the field scans where skyrmion phase is characterised by positive and negative peaks at skyrmion phase boundaries. Thus it seems, that there are two complementary methods using the same technique. With field scans, we can clearly identify the lower and upper phase boundaries whereas with the temperature scans, we can identify the Skyrmion phase region more clearly.

We first draw the phase digram in fig 4.14 and then categorize the temperature scans.
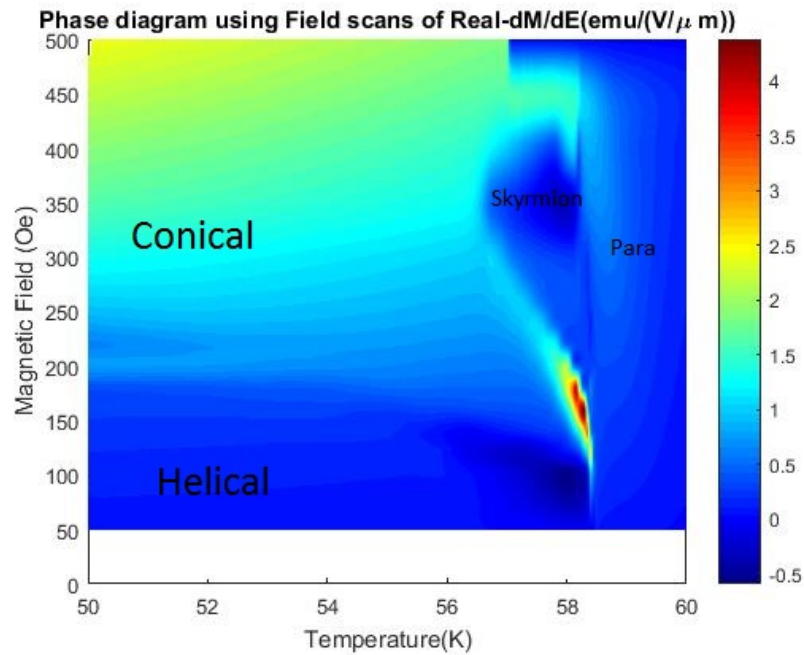
Figure 4.14 – Phase diagram from the temperature scans of magnetoelectric susceptibility measurements

We can clearly observe the skyrmion phase in the phase digram in fig 4.16. Also there is strong signature of conical to skyrmion phase transition near the lower boundary at low magnetic fields. .

Further I present some other temperature scans in fig 4.15-fig 4.18 which have been used to draw the phase diagram in fig 4.14.
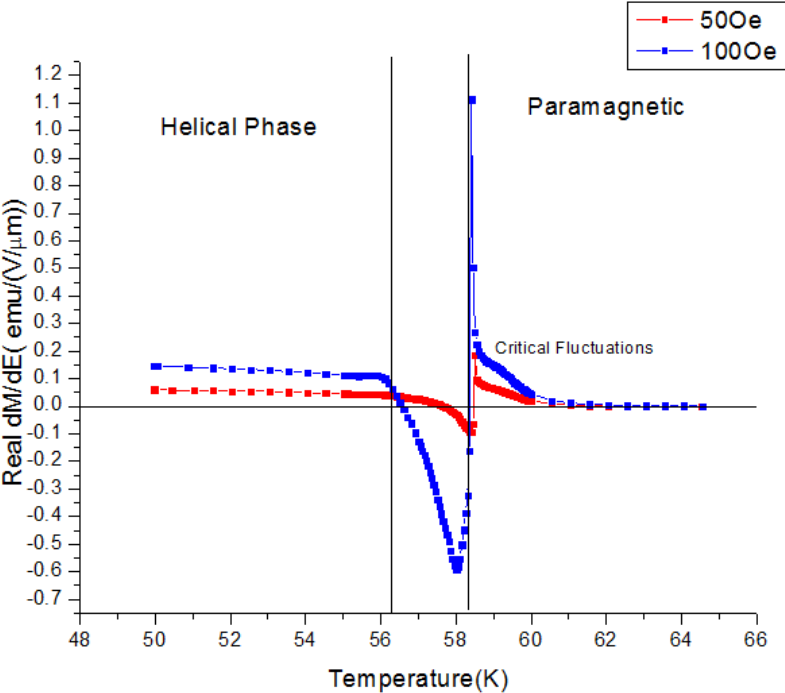
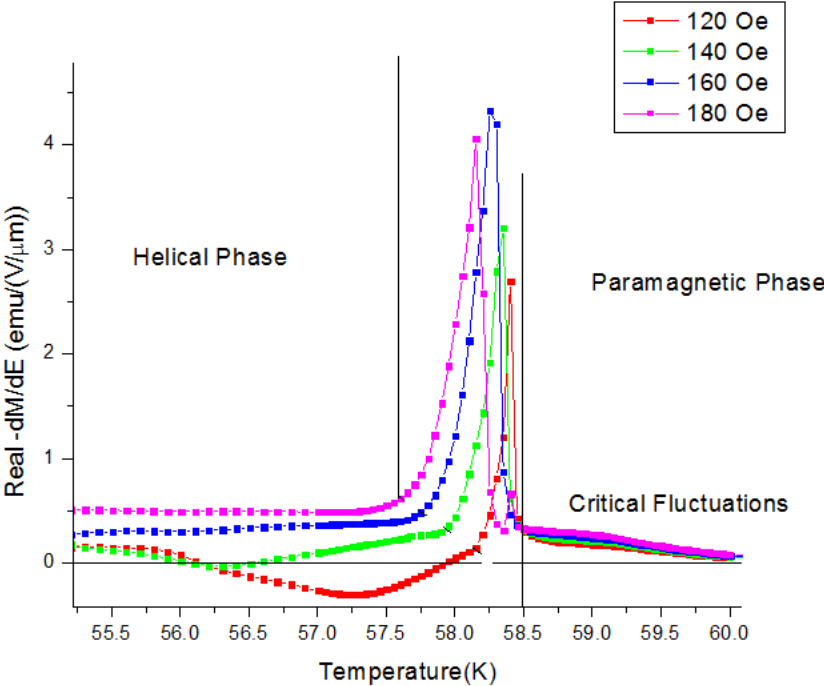Figure 4.15 – Temperature scans in the helical phase region

Figure 4.16 – Temperature scans showing helical phase region and helical to paramagnetic transition.
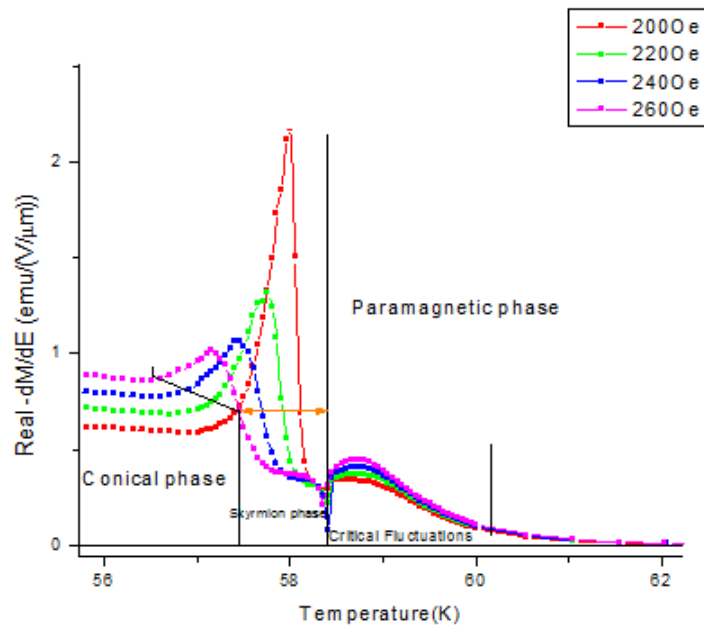
Figure 4.17 – Temperature scans showing conical phase region and skyrmion phase region
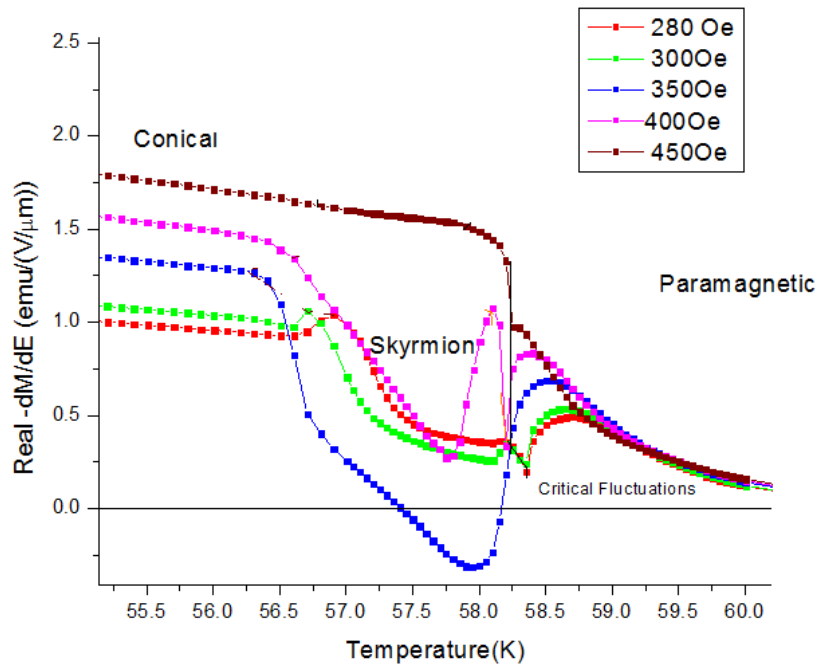
Figure 4.18 – Temperature scans showing conical phase region and broad skyrmion phase region.

37

The region of critical fluctuations in the paramagnetic phase has not been investigated thoroughly. Though they have been observed by neutron scattering technique in this and similar B20 compounds like MnSi. [19]

Electric field effect in 0.62 mm sample

dM/dE measurements were performed at DC electric fields of +220 V and -270 V but no appreciable change was observed in the dM/dE signal. The figure 4.19 illustrates this behaviour.
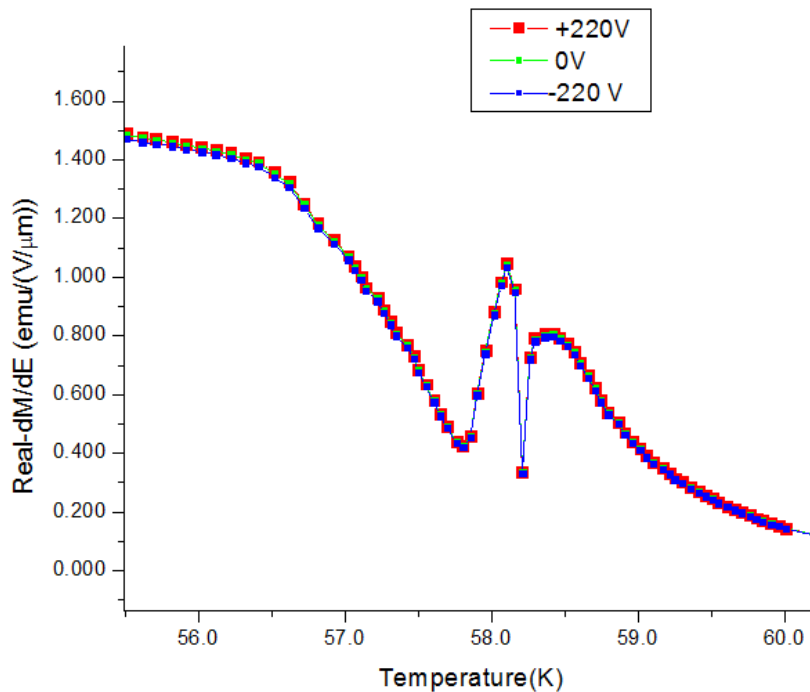

Figure 4.19 – The temperature scans show the magnetoelectric susceptibility responses at +220V, 0V and -250 V .

4.4 Magnetoelectric susceptibiltiy(dM/dE) measurements with different dc electric fields on 50 μm sample

Another sample of thickness 50 μm was prepared and it was glued to the substrate with GM varnish (approximately of same thickness on both sides). It was not possible to glue it with silver paint because of the some small cracks after polishing.

Field scans were performed to determine the phase boundaries with 0V, +220 V and -250V DC voltages. The excitation signal was 60V rms.

Figure 4.20 shows the phase corrected field scans at 55.3 K, 57.4 K and 58.0 K.

4.4. Magnetoelectric susceptibiltiy(dM/dE) measurements with different dc electric fields on 50 μm sample
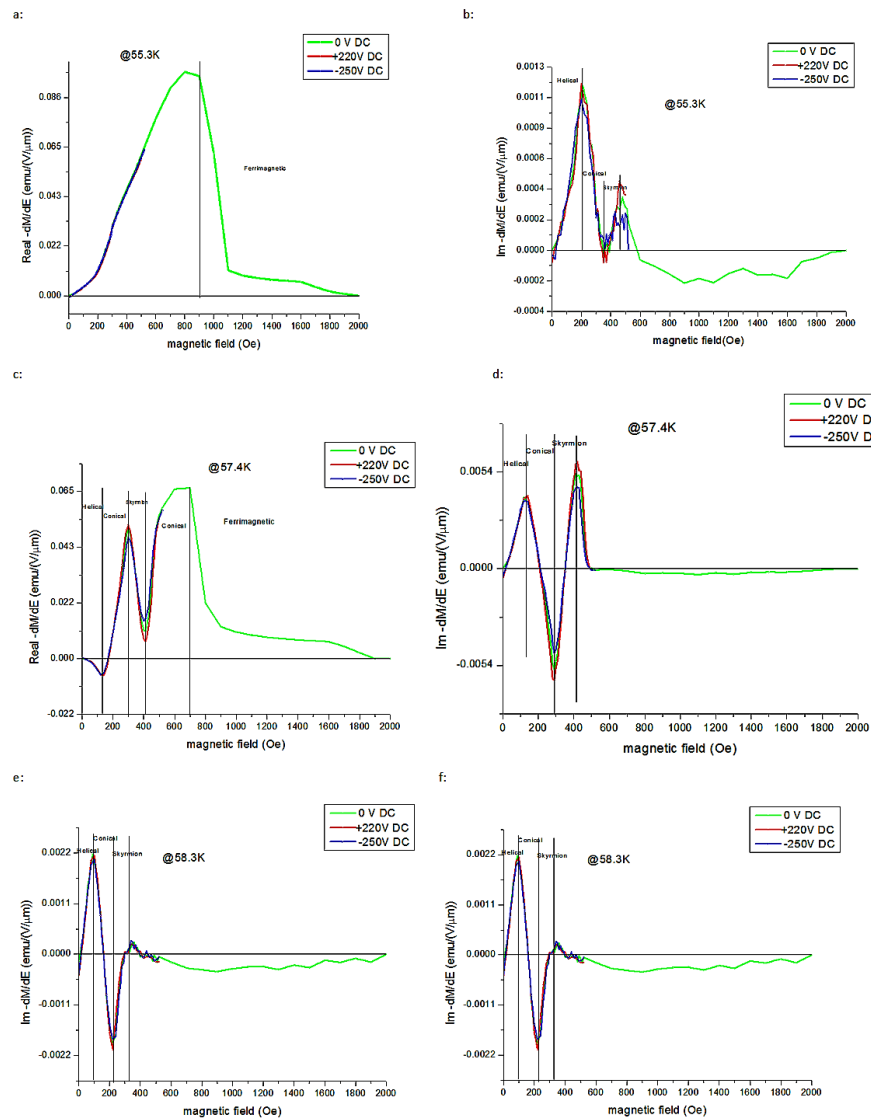

Figure 4.20 – Field scans at different temperature and applied DC electric fields. We can see that electric field effect is more pronounced at the Skyrmion phase boundaries.

We can see,in fig 4.20, that there is almost no skyrmion phase at 55.3K (within error bars) and there are prominent skyrmion phase boundaries visible at 57.4K which further diminish towards 58K.

We can observe certain trends from these field scans about electric field effect. First of all, the electric field effect is prominent only at the phase boundaries and almost negligible inside the phases. Second thing to note is that effect of electric field on helical to conical phase boundary is also very small compared to Skyrmion phase boundaries.Thus important thing to note is that magnetoelectric coupling can be increased or decreased on the skyrmion phase

boundaries by applying positive or negative DC electric field bias respectively.

One more thing to note is that the peaks representing phase boundaries are quite broad in compared to the peaks observed in field scans of 0.62 mm sample. The reason for this broadening is not known. One might suspect the thickness of sample to be responsible for this broadening but this is highly unlikely given that the periodicity of one Skyrmion unit cell in this material is 70 nm. Thus both the samples should represent 3-D behaviour .Thus cross over is not expected at this length.

Further we have done more field scans at different temperatures for +220V ,0V and -250V DC electric fields. We show the phase diagrams using these field scans in the fig 4.21-fig 4.23.
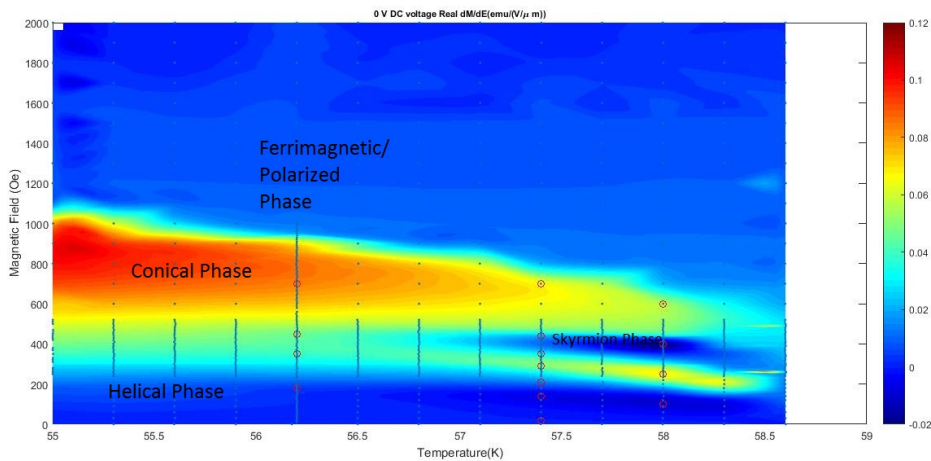

Figure 4.21 – Phase diagram at 0 V DC electric field. This also shows the conical to polarized phase transitions (the uppermost boundary),red large circles represent the points where DC electric field scans have been performed in next section.

4.4. Magnetoelectric susceptibiltiy(dM/dE) measurements with different dc electric fields on 50 μm sample
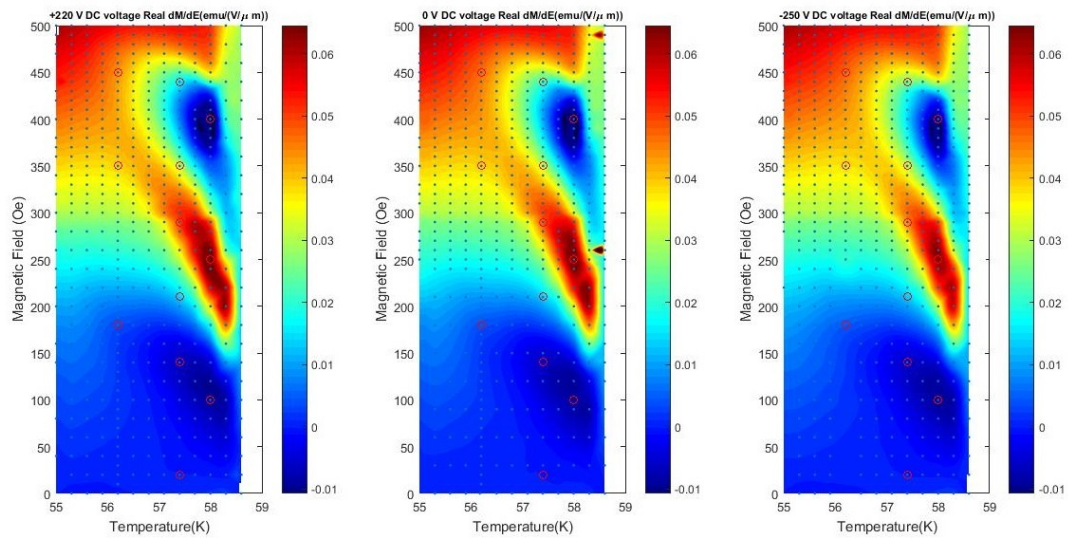

Figure 4.22 – Phase diagrams using real part of magnetoelectric susceptibility signal at +220V , 0V and -250V DC voltages. There is very small expansion of the phase boundary along the temperature axis in case of +220 V if compared to 0V and -250V. Black dots represent actual data points
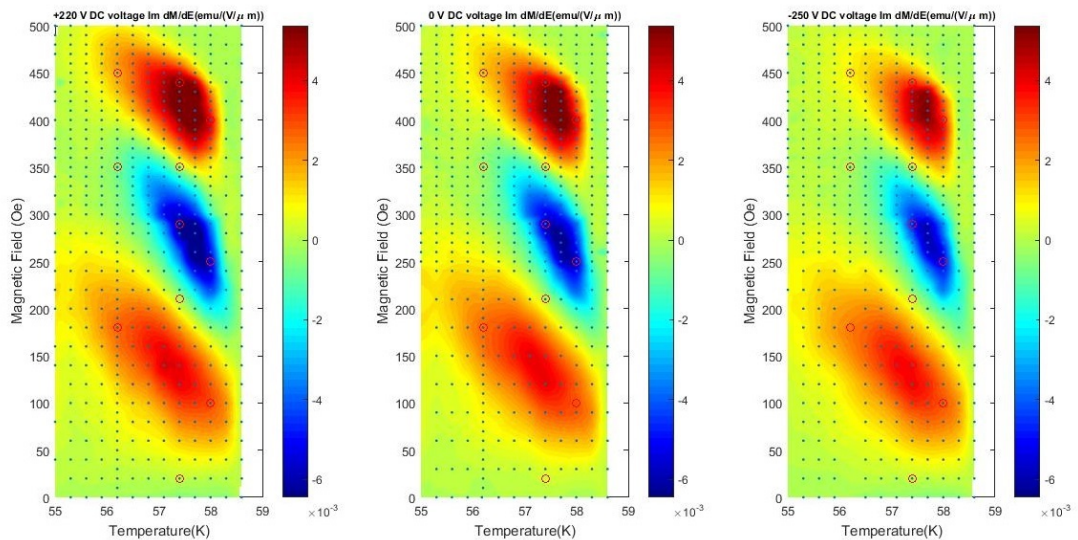

Figure 4.23 – Phase diagrams using Im part of magnetoelectric susceptibility signal at +220V , 0V and -250V DC voltages. There is very small expansion of the phase boundary along the temperature axis in case of +220 V if compared to 0V and -250V

We also draw the difference plots for phase diagrams of different electric fields to know the electric field effect,fig 4.24- fig 4.25.
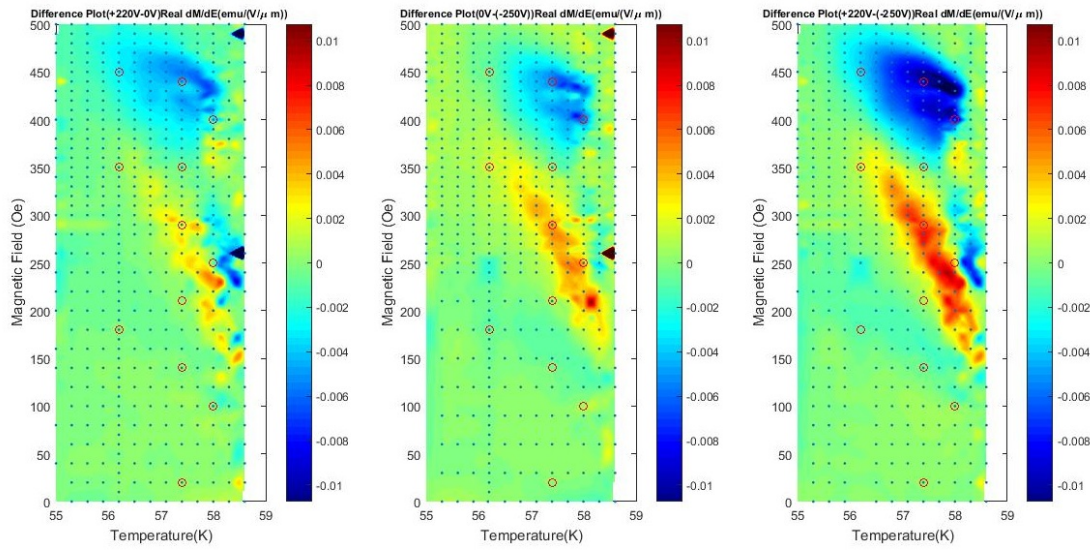
Figure 4.24 – Difference plots showing the electric field effect for real part of dM/dE signal. The effect is very strong on the skyrmion phase boundaries where as it is very small at helical to conical phase boundary and negligible inside the different phases
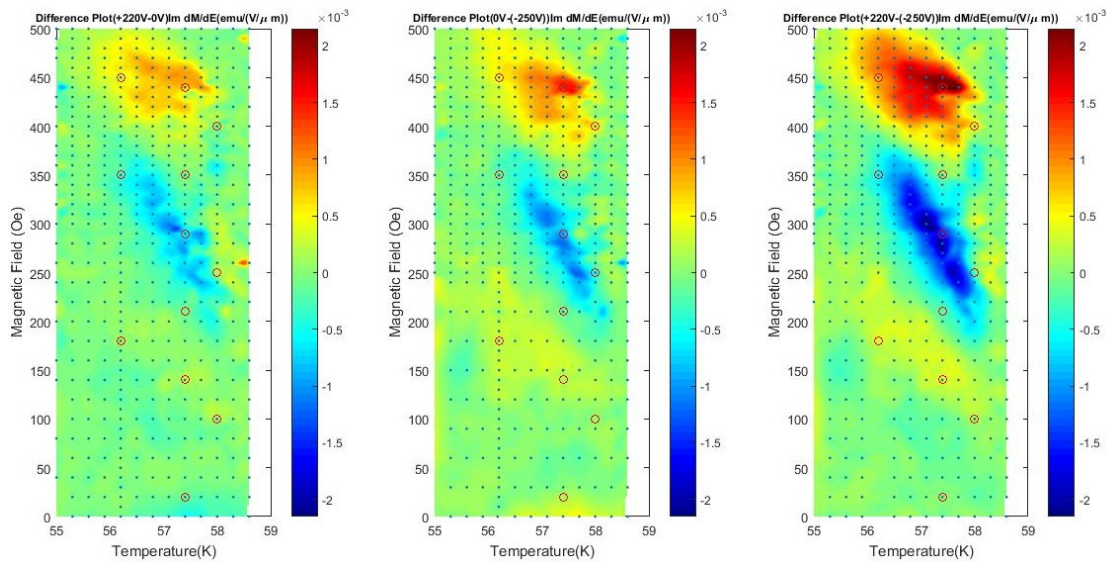

Figure 4.25 – Difference plots showing the electric field effect for Imaginary part of dM/dE signal. The effect is very strong on the skyrmion phase boundaries where as it is very small at helical to conical phase boundary and negligible inside the different phases

From the difference plots, it is clear that effect of electric field on magnetoelectric susceptibility signal is pronounced only on the lower and upper skyrmion phase boundaries. There is very small effect on helical to conical phase boundary. There is negligible effect of electric field inside the Skyrmion phase.

We see, form the phase diagrams at 220 V DC and -250 V DC , there is small expansion in the phase boundary along the temperature axis .This is in the range of 0.3K-0.4K. This is very small expansion even at the similar electric field as reported by Okamura et al. using AC magnetic susceptibility and microwave spectroscopy [10]. From the field scans as well as from the phase diagrams, we also observe no shift in the phase boundary in the field axis which is in contrast to that reported by [10]. We also performed one temperature scan for observing the electric field effect at 400 Oe magnetic field. It is shown in fig 4.26.
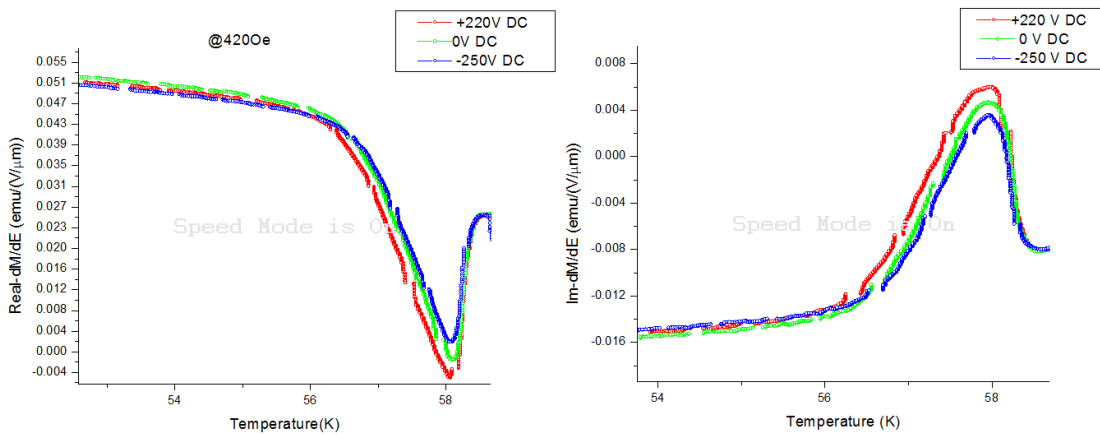

Figure 4.26 – Temperature scan at different DC fields for illustrating the electric field effect

4.5 DC electric field scans

Further to know the electric field dependence at various phase boundaries, the dc electric field scans were performed at the points marked with round red circles on phase diagrams.

First we qualitatively analyse DC field scans at the same temperatures as shown in fig 4.27.
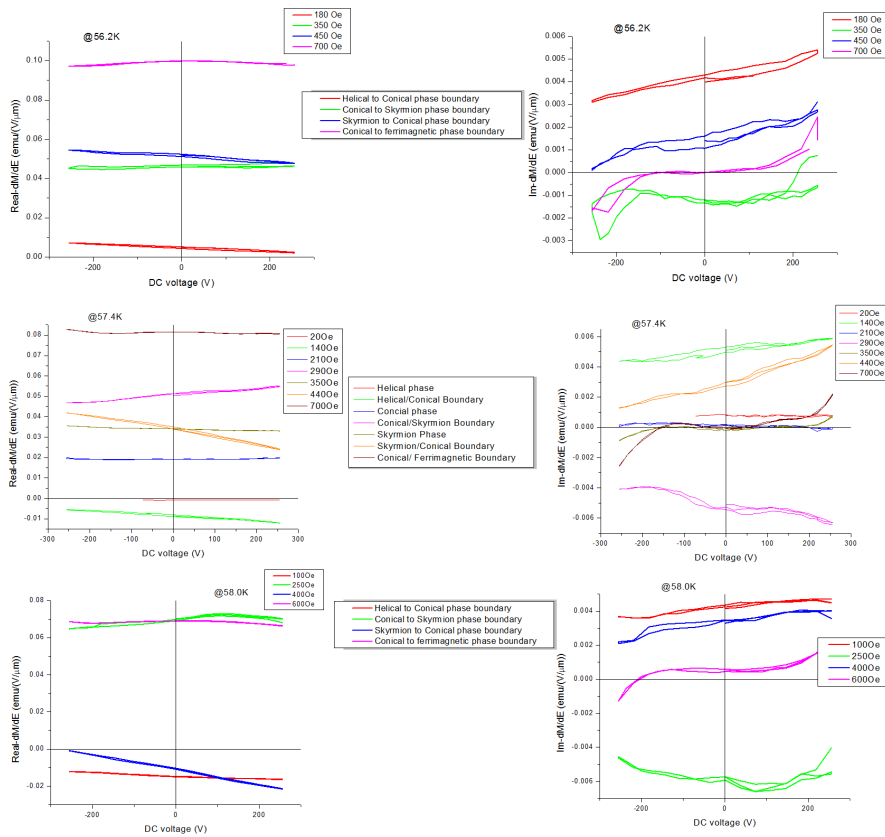
Figure 4.27 – DC Electric field scans of dM/dE signal at various field and temperatures for qualitative and quantitative comparison of electric field effect at different phase boundaries and inside various phases.

We observe, from dc scans at 56.2K,in fig 4.27 on , that electric field has same dependence at helical to conical phase boundary (180Oe) and Skyrmion to conical phase boundary (450Oe).The real part of dM/dE signal has linear dependence whereas imaginary part has small nonlinear dependence at high fields

DC scan at 350Oe has very small electric field dependence for small fields and non-linear dependence for high electric fields one interesting point to note that most of the DC field scans have symmetric dependence about zero electric field whether linear or non-linear response.

From the DC field scans at 57.4K, It is quite clear that electric field has no effect inside the helical, conical or Skyrmion phases for real part of dM/dE signal. Though there can be seen small non-linear dependence in case of imaginary part of dM/dE signal inside the Skyrmion phase at high electric field (57.4K,350Oe). We can clearly observe largest field dependence on upper Skyrmion boundary (440Oe)

Even from the DC field scans at 58.0K, it is clear that largest electric field effect can be observed at upper Skyrmion boundary. Also we can observe that there is large hysteresis observed at

upper skyrmion boundary at 56.2K (450Oe).

Now we proceed to quantify the electric field effects at the same boundaries in fig 4.28-fig 4.31.
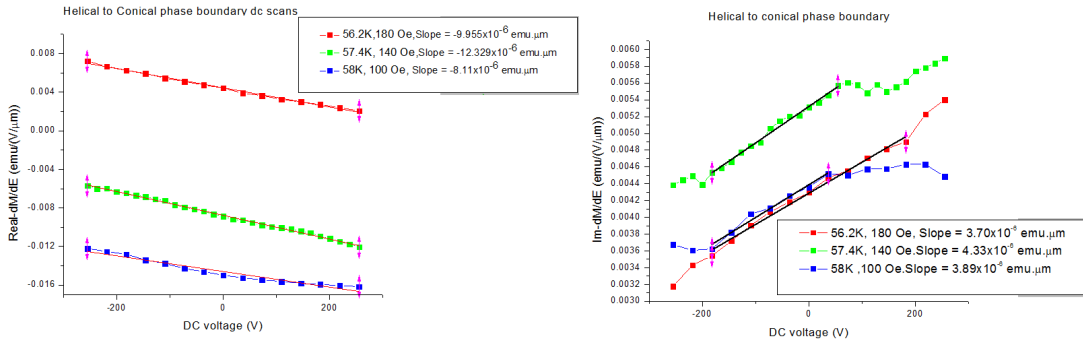

Figure 4.28 – DC field scans showing the electric field effect at 3 temperature.magnetic field conditions which lie at the helical to conical phase boundary.We observe the linear dependence in all the three cases

We see, in fig 4.28, that there is more electric field effect at 57.4K for the helical to conical phase boundary compared to dc scans at 56.2K and 58 K.
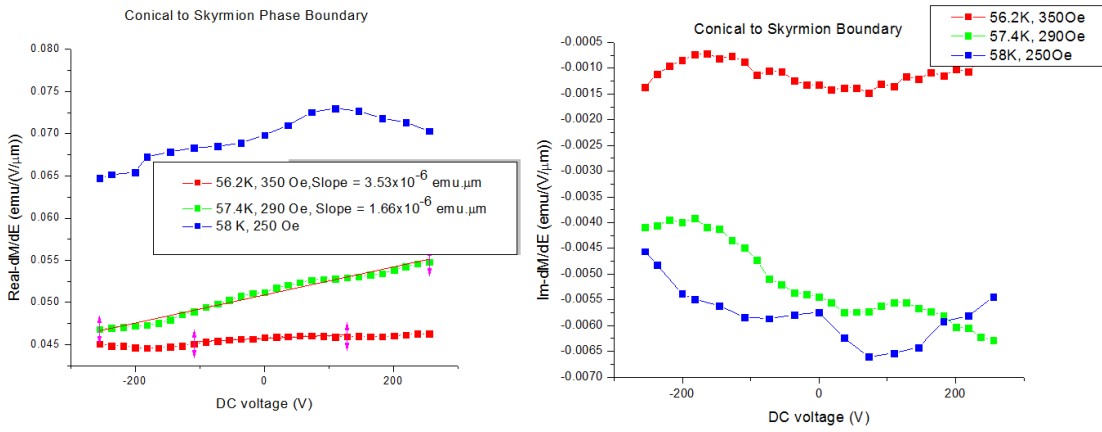

Figure 4.29 – DC electric field effect at conical to Skyrmion phase boundary

For lower boundary of Skyrmion phase,in fig 4.29, electric field effect is more pronounced at 57.4K (middle of the boundary) whereas electric field effect is not linear for 58K. This may be because of fluctuations near the paramagnetic phase boundary.
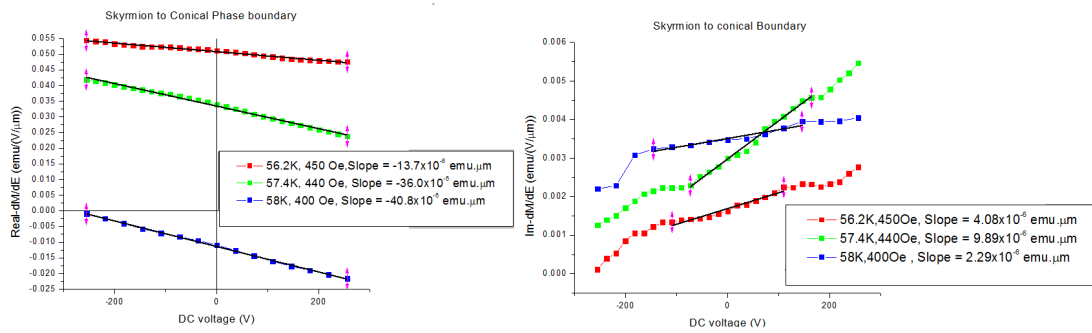
Figure 4.30 – DC electric field effect at skyrmion to conical phase boundary,Linear fitting shows the large electric field effect at 58 K compared to 56.2K

For the upper boundary of Skyrmion phase,in fig 4.30, The electric field dependence of real part of dM/dE signal is linear and increases from lower temperature side to upper temperature side. Though Imaginary part of dM/dE signal is non-linear at the high fields. Also the electric field effect is more at 57.4K compared to other two 56.2K and 58K. This is in contrast to the observed effect in real-dM/dE signal.
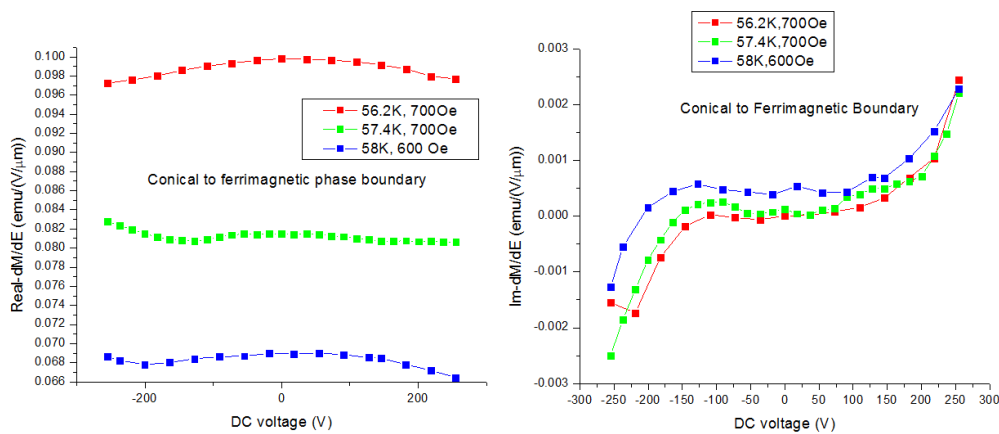

Figure 4.31 – DC electric field effect at conical to ferrimagnetic phase boundary

For the conical to ferrimagnetic phase boundary,in the fig 4.31, there is very small electric field dependence at all three temperatures. Though imaginary part of dM/dE signal shows a symmetric non-linear response for all three scans.

Thus, we can say that electric field has similar effect on the phase boundaries. Also Upper part of Skyrmion boundary shows most linear response with respect to electric field.The reasoning for some non-linear but symmetric responses in some scans is not clear and needs more investigation.

Now we summarize the results in phase diagram in fig 4.32

46
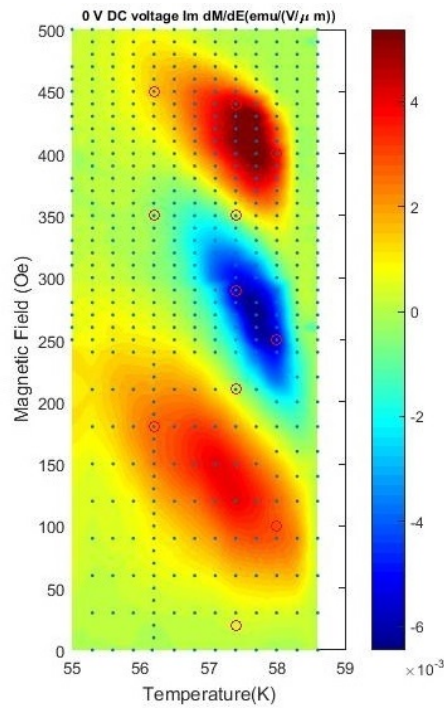
For the points in side red shaded region :: $\dfrac{d(\frac{dM}{dE}(Real))}{dE} < 0, \dfrac{d(\frac{dM}{dE}(Imaginary))}{dE} > 0$

For the points in side blue shaded region :: $\dfrac{d(\frac{dM}{dE}(Real))}{dE} > 0, \dfrac{d(\frac{dM}{dE}(Imaginary))}{dE} \sim Nonlinear\ response$

For the points in side green shaded region :: $\dfrac{d(\frac{dM}{dE}(Real))}{dE} \sim 0, \dfrac{d(\frac{dM}{dE}(Imaginary))}{dE} \sim 0\ for\ small\ E\ and\ Nonlinear\ for\ large\ E$

Figure 4.32 – Phase diagram with the summary below to identify the regions of similar electric field dependence

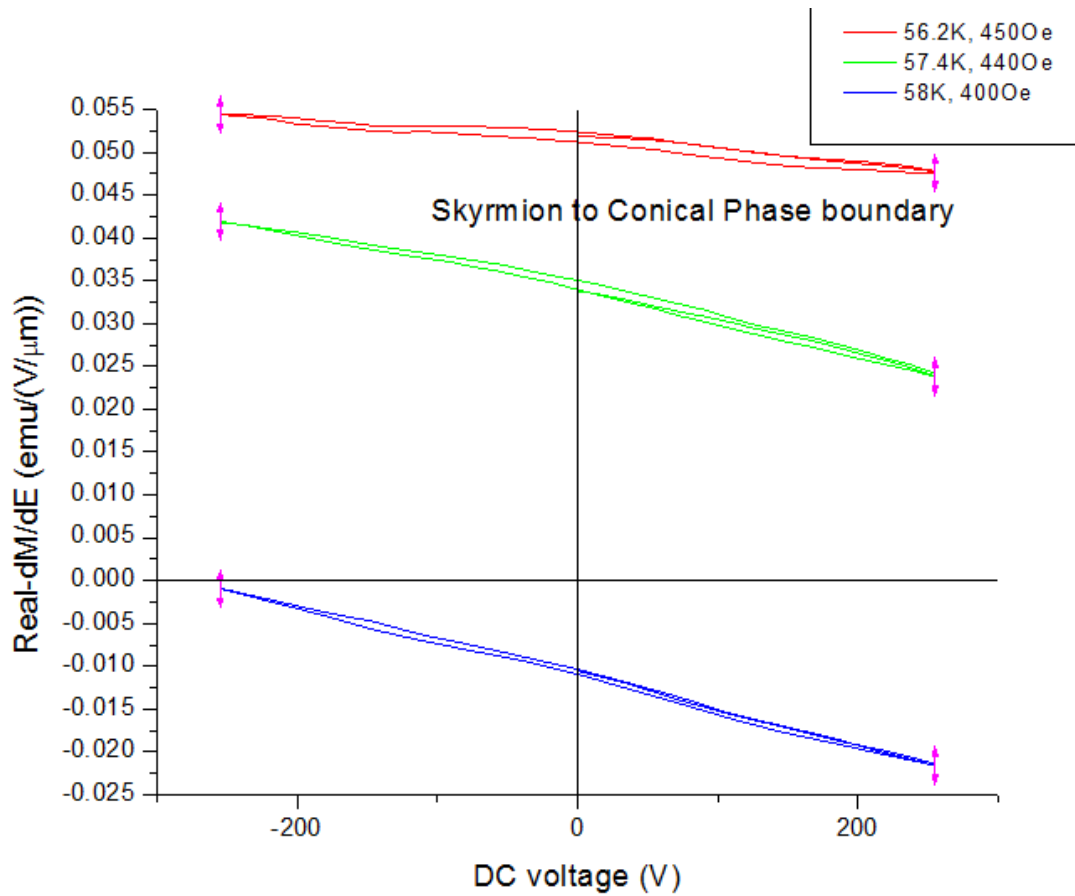## 4.6 Hysteresis Effect at upper Skyrmion boundary

Figure 4.33 – Hysteresis effect comparison at upper Skyrmion boundary. There is more hysteresis effect at 56.2 K compared to 57.4K or 58 K

We can clearly observe, in fig 4.33, that Hysteresis effect is more for 56.2 K and lowest at 58K. This is in contrast to the electric field effect which is more for 58 K compared to 56.2 K.

Though Hysteresis observed in the dM/dE signal is very small as compared to the Hysteresis observed in the AC magnetic susceptibility signal as reported by [10].

4.7 Metastable Skyrmion phase at low temperatures

Another aim of the thesis was to observe the metastable skyrmion state at lower temperatures by either magnetoelectric cooling or by quenching (cooling with certain temperature rate). The motivation for these studies came from the recent study by Okamura et al [10], where they could create the metastable states by doing the magnetoelectric cooling as shown in the figure 4.34. But there could not be observed any such phenomenon in our experiment. Figure 4.35

shows two different continuous temperature scans at different cooling rates in order to study metastability.
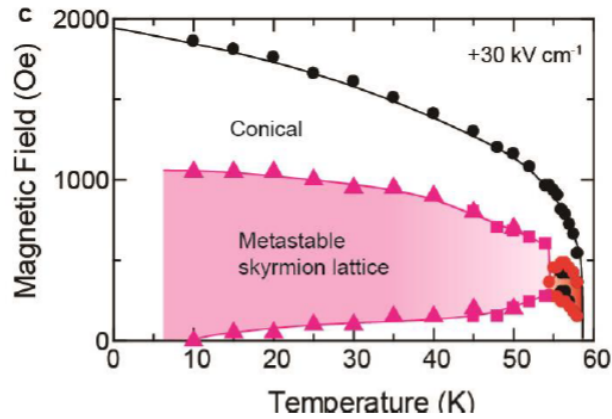

Figure 4.34 – metastable state created by magnetolelectric cooling . Figure taken from [10]
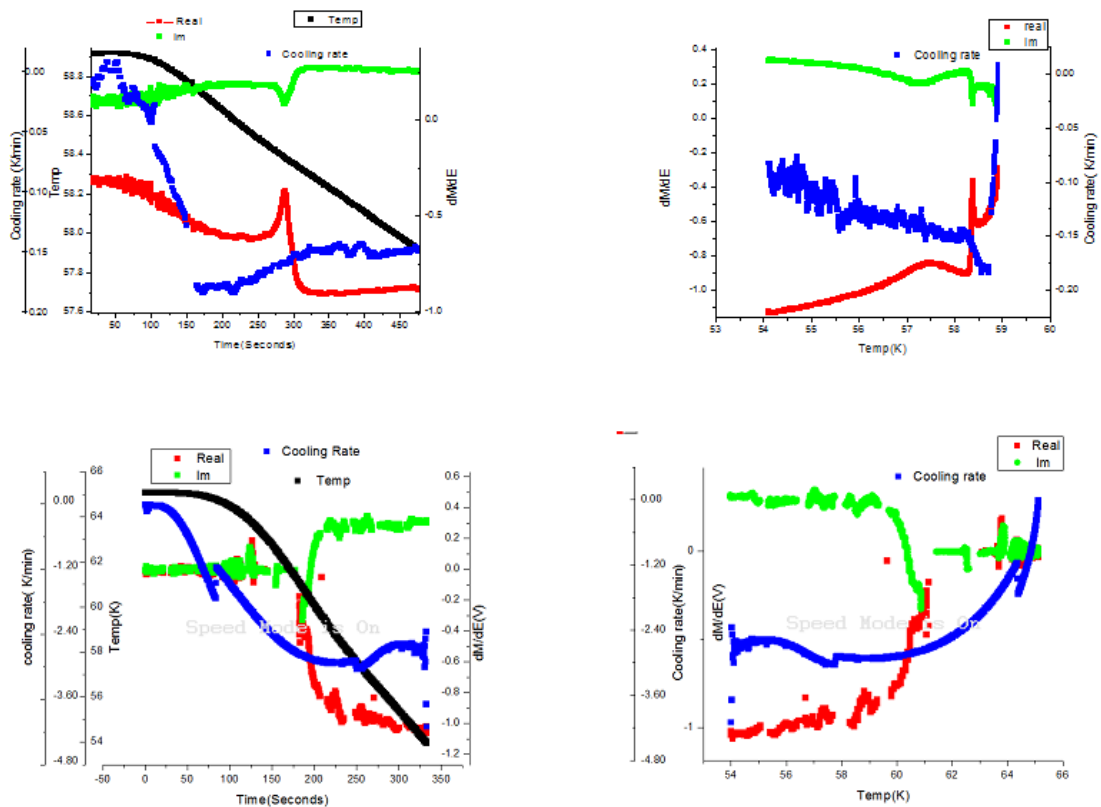

Figure 4.35 – Continuous temperature scans at different cooling rates for the purpose of creating metastable states. No feature is seen describing the creation of metastable states at low temperatures

We can observe that Skyrmion phase can not be precisely identified because of lag between actual sample temperature and temperature at sensor B. Though if we assume, as evident that cooling rate is constant in the Skyrmion phase region, then we can comapre the Skyrmion phase region. We see that the skyrmion region in the scan with cooling rate of 0.1 K/min is small in compared the temperature scan at cooling rate of 3 K/min but because of lack of data, we can't make any conclusions about the crating the metastable phase. . Though it is also evident that Skyrmion phase does not persist down to low temperatures as mentioned by Okamura et al [10].

5 Conclusion

In the present thesis, I addressed the problem of manipulating the Skyrmion Phase by applying the DC electric field. It was found , from DC field scans, that there is no cut-off for the electric field effect and it is continuous. But it depends on the instrument sensitivity that how much field is required to observe the comparable difference between the dM/dE signal with and without application of DC electric field. This is evident from the fact, we were not able to see the electric field effect in 0.62 mm sample because of small electric field.

Further, it was found that DC electric field effects, on dM/dE signal, are more pronounced at the phase boundaries and decrease inside any phase . Also, it affects the upper skyrmion boundary most.

No shift was observed in the peaks of dM/dE signal along magnetic field by applying the DC electric field. This is in contrast to the recent study [10] in which there has been observed change in the phase boundary along magnetic field (contraction/expansion). We need more investigation to this fact because this might be because of broadened peaks in the sample.

Though we were able to observe very small shift in the phase boundary along the temperature axis, This is very small in compared to given in [10].

It was found that electric field has similar effects on same boundaries. Hysteresis effect in DC electric field scan is more pronounced at low temperature side of upper Skyrmion boundary (56.2K, 450 Oe) compared to hysteresis at 58K and 400 Oe.

Mangetolectric susceptibility presents better way of studying phase transitions in these materials compared to magnetization measurements.

Few important points which need the more investigation are critical fluctuations near paramagnetic phase boundary, Broadening of peaks in the 50 μm sample compared to that observed in 0.62 mm sample and nonlinear response in the high electric fields inside the Skyrmion phase

Also we were not able to observe the metastable skyrmion state at low temperature either by

magnetoelectric cooling procedure or by quenching of temperature with cooling rates of 0.1 K/min or 3K/min.

Further I hope that findings in this thesis will be valuable for future plans to study the physics in this material.
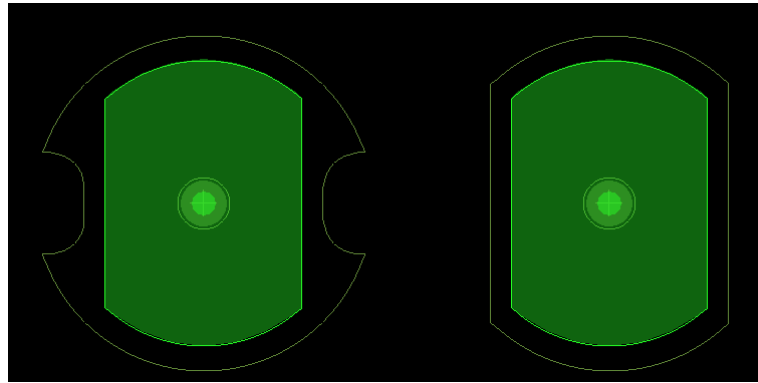
A | An appendix

Figure A.1 – PCB Design of sample holder parts.These parts are used to provide support and make the electric contacts with the sample. Both parts are coated with 35 μm thick copper layer. One of the substrates can be glued to sample after one side polish of sample and then it will be easy to polish other side without possibly breaking the sample.
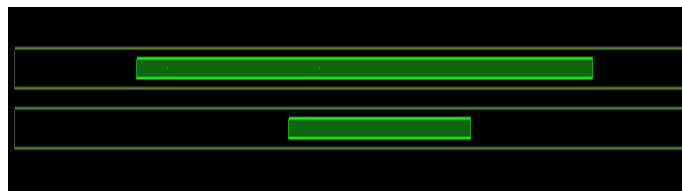

Figure A.2 – PCB Design of sample stick with 35 μm thick coating of copper to make electrical connection with the sample holder and hold it at place.
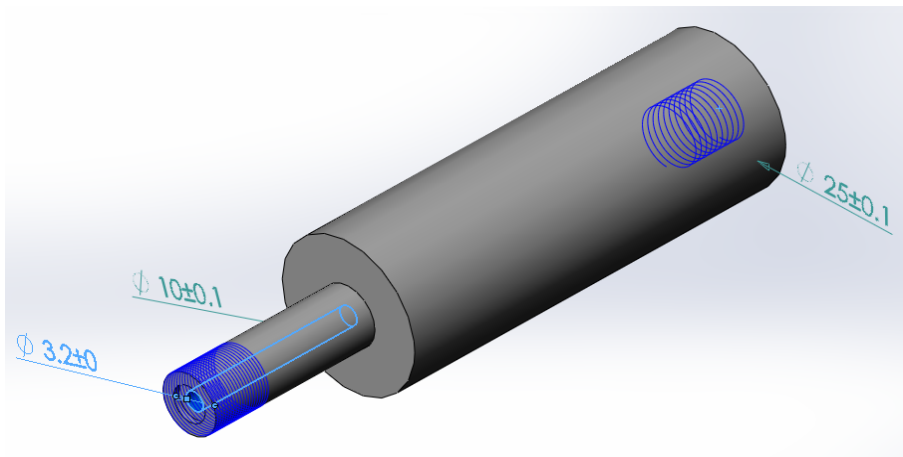
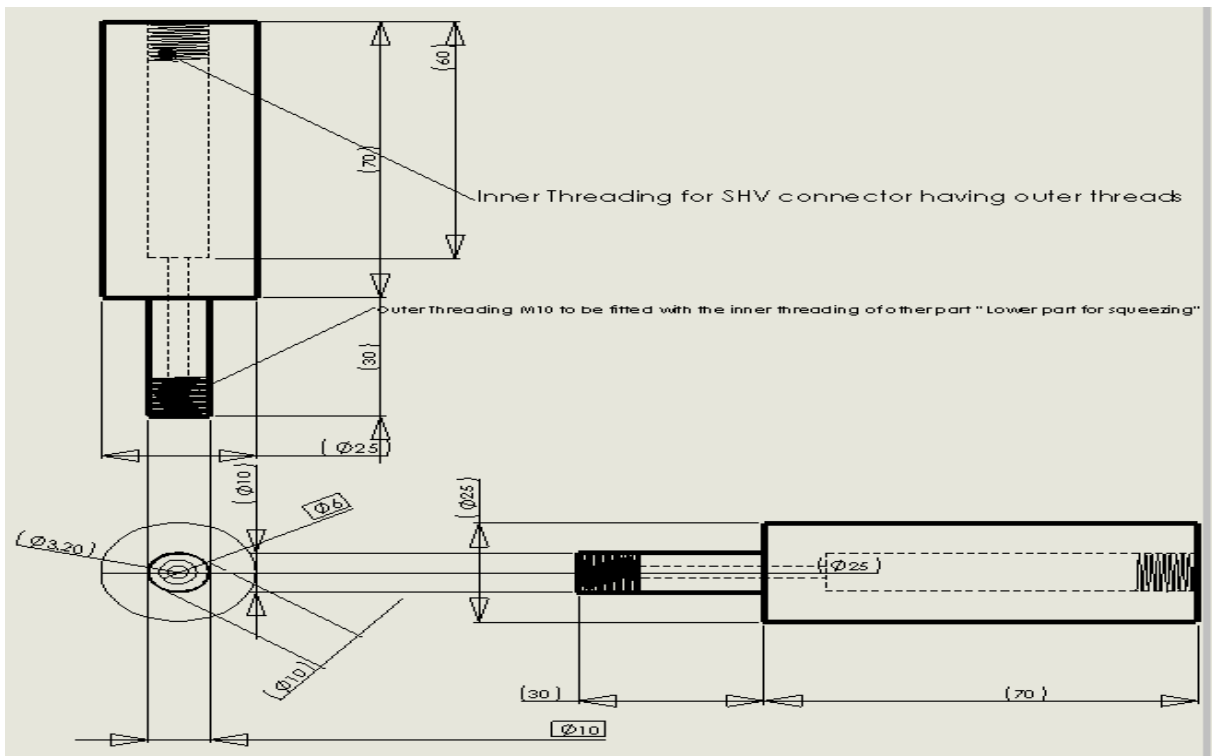Figure A.3 – 3-D design of main body of upper detachable part, all dimensions are in mm.

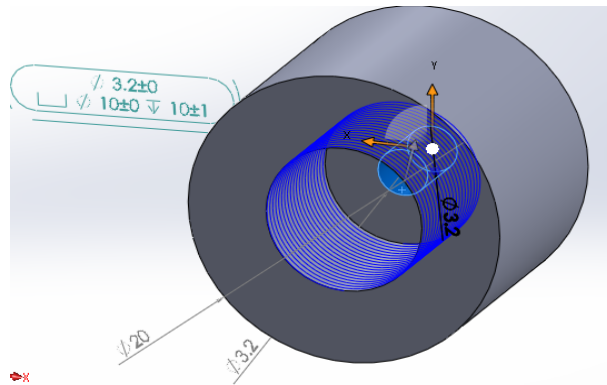Figure A.4 – 2-D schematic of main body of upper detachable part of sample probe, All dimensions are in mm.

Figure A.5 – 3-D design of the Squeezing part to hold the connector on the sample probe and air seal to avoid any air going through the tube.
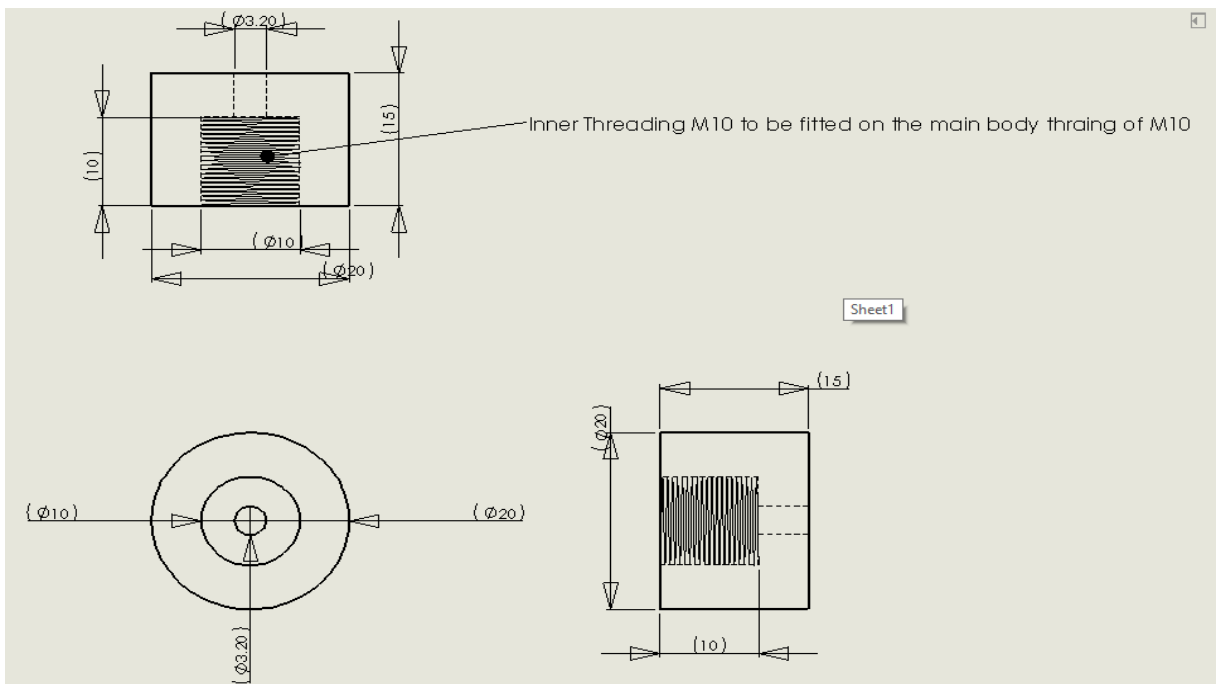

Inner Threading M10 to be fitted on the main body thraing of M10

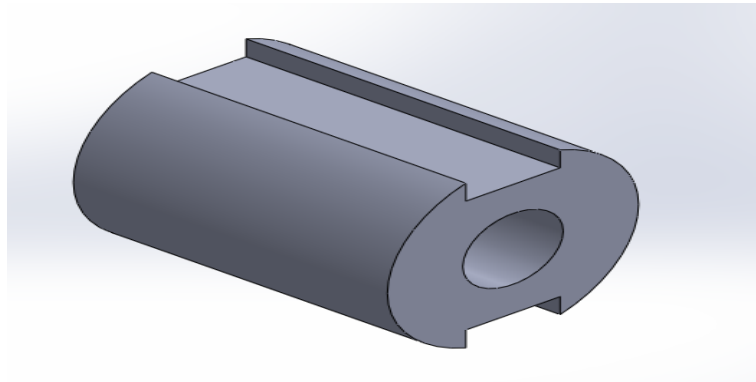Figure A.6 – 2-D schematic of the Squeezing part to hold the connector on the sample probe

Figure A.7 – 3-D design of brass piece to hold the PCB stick with sample probe. This is attached permanently to sample probe
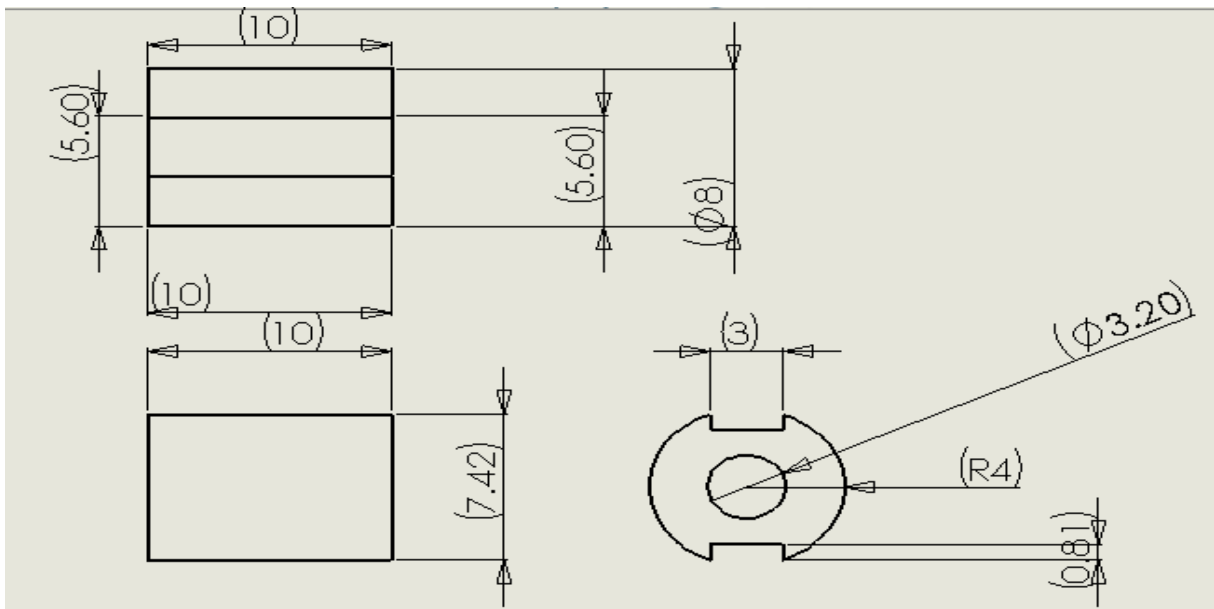

Figure A.8 – 2-D schematic of brass piece to hold the PCB stick

Bibliography

[1] S. Seki, X. Z. Yu, S. Ishiwata, and Y. Tokura. Observation of skyrmions in a multiferroic material. *Science*, 336(6078):198–201, apr 2012.

[2] Shinichiro Seki and Masahito Mochizuki. *Skyrmions in Magnetic Materials*. Springer International Publishing, 2016.

[3] Xichao Zhang, Motohiko Ezawa, and Yan Zhou. Magnetic skyrmion logic gates: conversion, duplication and merging of skyrmions. *Scientific Reports*, 5:9400, mar 2015.

[4] N. Romming, C. Hanneken, M. Menzel, J. E. Bickel, B. Wolter, K. von Bergmann, A. Kubetzka, and R. Wiesendanger. Writing and deleting single magnetic skyrmions. *Science*, 341(6146):636–639, aug 2013.

[5] Jing Xia, Yangqi Huang, Xichao Zhang, Wang Kang, Weiwei Wang, Chentian Zheng, Xiaoxi Liu, Weisheng Zhao, and Yan Zhou. Magnetic skyrmion transistor operated with microwaves.

[6] Xichao Zhang, G. P. Zhao, Hans Fangohr, J. Ping Liu, W. X. Xia, J. Xia, and F. J. Morvan. Skyrmion-skyrmion and skyrmion-edge repulsions in skyrmion-based racetrack memory.

[7] A. A. Omrani, J. S. White, K. Prša, I. Živković, H. Berger, A. Magrez, Ye-Hua Liu, J. H. Han, and H. M. Rønnow. Exploration of the helimagnetic and skyrmion lattice phase diagram in cu 2 OSeO 3 using magnetoelectric susceptibility. *Physical Review B*, 89(6), feb 2014.

[8] Arash Alahgholipour Omrani. *Nanofabricated Devices based on Intrinsically Layered Correlated Electron Materials*. PhD thesis, 2013.

[9] Jan-Willem G. Bos, Claire V. Colin, and Thomas T. M. Palstra. Magnetoelectric coupling in the cubic ferrimagnet cu 2 OSeO 3. *Physical Review B*, 78(9), sep 2008.

[10] Y. Okamura, F. Kagawa, S. Seki, and Y. Tokura. Transition to and from the skyrmion lattice phase by electric fields in a magnetoelectric compound. *Nature Communications*, 7:12669, sep 2016.

[11] J S White, I Levatić, A A Omrani, N Egetenmeyer, K Prša, I Živković, J L Gavilano, J Kohlbrecher, M Bartkowiak, H Berger, and H M Rønnow. Electric field control of the

skyrmion lattice in cu 2 OSeO 3. *Journal of Physics: Condensed Matter*, 24(43):432201, oct 2012.

[12] S. Seki, S. Ishiwata, and Y. Tokura. Magnetoelectric nature of skyrmions in a chiral magnetic insulator cu 2 OSeO 3. *Physical Review B*, 86(6), aug 2012.

[13] Naoto Nagaosa and Yoshinori Tokura. Topological properties and dynamics of magnetic skyrmions. *Nature Nanotechnology*, 8(12):899–911, dec 2013.

[14] Ye-Hua Liu and You-Quan Li. Dynamics of magnetic skyrmions. *Chinese Physics B*, 24(1):017506, jan 2015.

[15] Ye-Hua Liu, You-Quan Li, and Jung Hoon Han. Skyrmion dynamics in multiferroic insulators. *Physical Review B*, 87(10), mar 2013.

[16] Shi-Zeng Lin and Satoru Hayami. Ginzburg-landau theory for skyrmions in inversion-symmetric magnets with competing interactions.

[17] Jayaraman Rajeswari, Ping Huang, Giulia Fulvia Mancini, Yoshie Murooka, Tatiana Latychevskaia, Damien McGrouther, Marco Cantoni, Edoardo Baldini, Jonathan Stuart White, Arnaud Magrez, Thierry Giamarchi, Henrik Moodysson Rønnow, and Fabrizio Carbone. Filming the formation and fluctuation of skyrmion domains by cryo-lorentz transmission electron microscopy. *Proceedings of the National Academy of Sciences*, 112(46):14212–14217, nov 2015.

[18] Ye-Hua Liu, Jung Hoon Han, A. A. Omrani, H. M. Rønnow, and You-Quan Li. Theory of magneto-electric susceptibility in multiferroic chiral magnets.

[19] Koya Makino, Johannes D. Reim, Daiki Higashi, Daisuke Okuyama, Taku J. Sato, Yusuke Nambu, Elliot P. Gilbert, Norman Booth, Sinichiro Seki, and Yoshinori Tokura. Thermal stability and irreversibility of skyrmion-lattice phases in cu_2oseo_3.